國 立 交 通 大 學

機械工程學系

博 士 論 文

探討單壁奈米碳管複合材料之機械性質

Investigating Mechanical Properties of

Single-Walled Carbon Nanotubes Nanocomposites

研 究 生 ：曾世華

指導教授 ：蔡佳霖 博士

中 華 民 國 壹 百 年 壹 月

探討單壁奈米碳管複合材料之機械性質

Investigating Mechanical Properties of
Single-Walled Carbon Nanotubes Nanocomposites

研 究 生：曾世華　　　　　　　　　Student：Shi-Hua Tzeng

指導教授：蔡佳霖　　　　　　　　　Advisor：Jia-Lin Tsai

國　立　交　通　大　學

機　械　工　程　學　系

博　士　論　文

A Dissertation

Submitted to Department of Mechanical Engineering

College of Engineering

National Chiao Tung University

in Partial Fulfillment of the Requirements

for the Degree of

Doctor of Philosophy

in

Mechanical Engineering

January 2011

Hsinchu, Taiwan, Republic of China

中 華 民 國 壹 百 年 壹 月

探討單壁奈米碳管複合材料之機械性質

研究生：曾世華　　　　　　　　　指導教授：蔡佳霖 博士

國立交通大學機械工程學系

摘要

　　本研究利用多尺度模擬方法探討以單壁奈米碳管為加強材之聚亞醯胺奈米複合材料之機械性質，並且利用分子動力學探討奈米碳管嵌入聚亞醯胺分子所構成之奈米複合材料，在其遭受負荷時奈米碳管上所產生的應力分佈。奈米碳管之分子結構為一中空圓柱，利用一橫向等向性之實心圓柱結構模擬奈米碳管，而等效實心圓柱結構之機械性質可利用能量等效之概念獲得，藉由分子動力學建立奈米碳管/聚醯亞胺奈米複合材料，進而計算出奈米碳管與週遭聚醯亞胺之間的非鍵結間距以及非鍵結能。假設正交化非鍵結能與界面層作用力相關，則可在奈米碳管以及高分子之間考慮一等效界面層，其中尺寸為非鍵結間距，而彈性勁度則可藉由正交化非鍵結能得到。最後利用三層界面層微觀力學模型，分別考慮等效實心圓柱，高分子基材以及等效界面層可預測奈米複合材料的機械性質。結果可發現利用三界面層微觀力學模型預測奈米複合材料的軸向機械模數與分子動力學結果一致，且都與傳統之混合原則結果相符。而在橫向部分，三層界面層微觀力學模型比傳統微觀力學模型更能夠預測出奈米複合材料的橫向模數隨著奈米碳管半徑增加而下降之現象。

　　利用分子動力學探討奈米碳管嵌入聚亞醯胺分子所構成之奈米複合材料，在其遭受負荷時奈米碳管上所產生的應力分佈。基本上，負荷傳遞效率在奈米複合材料的機械性質上扮演著重要角色。藉由奈米碳管上的應力分佈情形，可以了解奈米加強材及其周遭聚亞醯胺基材之間的負荷傳遞效率。考慮奈米碳管及

聚亞醯胺基材之間三種不同的原子作用力，分別為凡得瓦作用力、表面改質之奈米碳管以及共價鍵結合之界面層。當奈米複合材料遭受負荷時，可利用原子等級應力公式以及能量公式推導計算嵌入其內之奈米碳管的應力分佈，進而可定義負荷傳遞至奈米碳管的效率。結果發現表面改質過的奈米碳管可以使負荷更容易由聚亞醯胺分子傳遞至奈米碳管，使得奈米複合材料有較好的機械性質。此外，若奈米碳管的表面沒改質劑時，界面層僅存在凡得瓦作用力，因而導致較差的負荷傳遞效率。因此，在製作以奈米碳管為加強材之奈米複合材料時，表面改質的奈米碳管可以有效的改善奈米複合材料的負荷傳遞效率以及機械性質。

Investigating Mechanical Properties of Single-Walled Carbon Nanotube Nanocomposites

Student：Shi-Hua Tzeng   Adviser：Jia-Lin Tsai

Department of Mechanical Engineering
National Chiao Tung University

Abstract

The aim of thesis is to characterize the mechanical properties of single-walled carbon nanotubes (SWCNTs) reinforced with polyimide nanocomposites using a multi-scale simulation approach, and to investigate the stress distribution of SWCNTs embedded within polyimide nanocomposites under applied loading using molecular dynamics (MD) simulation. The hollow cylindrical molecular structures of SWCNTs were modeled as transversely isotropic solids, and the equivalent elastic properties of which were determined from the molecular mechanics calculations in conjunction with the energy equivalent concept. The molecular structures of the SWCNT/polyimide nanocomposites were established through MD simulation, from which the non-bonded gap as well as the non-bonded energy between the SWCNTs and the surrounding polyimide, were evaluated. The normalized non-bonded energy (non-bonded energy divided by surface area of the SWCNTs) was postulated to be correlated with the extent of interfacial interaction. An effective interphase was introduced between the SWCNTs and polyimide polymer to characterize the degree of non-bonded interaction. The dimension of the interphase was assumed to be equal to the non-bonded gap, and the corresponding elastic stiffness was calculated from the normalized non-bonded energy. The elastic properties of the SWCNT nanocomposites were predicted by a three-phase micromechanical model, in which the equivalent

solid cylinder of SWCNTs, polyimide matrix, and the effective interphase were included. Results indicated that the longitudinal moduli of the nanocomposites based on the three-phase model were in good agreement with those generated from MD simulation. Moreover, they are consistent with the conventional rule-of-mixtures predictions. In the transverse direction, the three-phase model is superior to the conventional micromechanical model because it is capable of predicting the dependence of the transverse modulus on the radii of nanotubes.

The stress distribution of SWCNTs embedded within polyimide nanocomposites subjected to applied loading was investigated using the MD simulation. The purpose of evaluating the stress distribution of SWCNTs is to characterize the loading transfer efficiency between the nano-reinforcement and surrounding polyimide matrix, which is an essential factor controlling the mechanical properties of nanocomposites. Three different interfacial adhesions between the SWCNTs and polyimide molecular were considered: the van der Waals (vdW) interaction, SWCNTs with surface modifications, and covalent bonds. The stress distribution of the SWCNTs was calculated using the atomic level stress formulation and by taking the derivative of the potential functions. The results revealed that when the SWCNTs surface was modified, a higher load transfer efficiency from the polyimide to the SWCNTs was observed, resulting in a higher modulus of the nanocomposites. Without surface modification on SWCNTs, the load transfer efficiency, which depends on the intensities of the vdW interactions, is relatively low. As a result, the surface modification on SWCNTs is an effective method to improve the load transfer efficiency as well as the modulus of the nanocomposites, and should be suggested in the fabrication of SWCNTs nanocomposites.

誌謝

在這漫長的研究生涯中，承蒙指導教授 蔡佳霖博士於學生碩士期間便不遺餘力的用心指導以及諄諄教誨，使我除了學術上的精進之外，也了解生活中待人處事應有的態度以及方法，讓我收穫良多。在此同時，感謝蔡佳霖實驗室的王漢偉學長、黃仁傑學長、陳奎漢學長、郭濬清學長、許世民學長以及盧廷鉅學長對我的關懷，使我備感窩心，祝福你們事業順利。另外也感謝齊揚凱、鄭伊烈、涂潔鳳、林奕安、張乃仁、謝孟哲、王泰元、徐政文、洪建峰、黃奕嘉、高菁穗、黃健洋、劉少淇、許嵩群及賴彥錕等諸位學弟妹在研究與生活中的陪伴，幫我克服許多的困難，其中齊揚凱、林奕安、謝孟哲、徐政文及高菁穗，因為有你們幫忙分擔實驗室的事務，使得我在博士生涯中能夠全心全力的投入於研究中，祝福你們學業以及工作順利。

在漫長的求學過程中，更要感謝家父曾永豐先生以及家母江鳳珠女士在背後的默默支持與體諒，使得孩兒能無後顧之憂的致力於研究，順利完成博士學位。也感謝聖慈陪伴我從大學到博士生涯，一路上因你使我的生命增添了許多色彩，也祝福你順利完成博士學位。

如今求學生涯即將告一段落，感謝一路上使我成長茁壯的人。

曾世華 謹誌
中華民國 100 年 1 月

Table of Contents

List of Tables

List of Figures

CHAPTER 1   INTRODUCTION

1.1 Background

Polymer nanocomposites are known to exhibit significantly enhanced mechanical, thermal, electrical, and magnetic properties compared to neat polymers. In recent years, with the increased applications of polymers and nanocomposites, the demand for high stiffness and low weight polymer nanocomposites is increasing. The small diameter, large aspect ratio, extremely high strength, and stiffness naturally make carbon nanotubes (CNTs) the most attractive reinforcement for polymer matrix composites. Iijima [1] first discovered CNTs using transmission electron microscopy in 1991. Since then, numerous studies have researched the structure, physical and mechanical properties of carbon nanotubes.

The structure of single-walled carbon nanotubes (SWCNTs) can be viewed as a graphene sheet rolled into a tube as shown in Fig. 1-1. The orientation along which nanotube is rolled is called chiral vector $\vec{C}_h$, and can be described by

$$\vec{C}_h = n\vec{a}_1 + m\vec{a}_2 \qquad (1.1)$$

where $\vec{a}_1$ and $\vec{a}_2$ are unit vectors for the hexagonal lattice of the graphene, n and m are two integers and the chiral angle θ is with respect to the x-axis. Based on the orientation of the rolling axis, carbon nanotubes can be divided into zigzag, armchair, and chiral typesFor the more general chiral type (n, m) we usually have n > m. The (n, n) structure is usually labeled the armchair type SWCNT and the (n, 0) structure is usually labeled the zig-zag type SWCNT. These different types of nanotube are shown in Fig. 1-2.

Numerous micromechanical models have been developed to predict the macroscopic behavior of polymeric composite materials typically reinforced with carbon or glass fibers [2]. However, for nanostructured materials such as CNTs, the atomic size scale may lead to inaccurate continuum modeling. To try to understand the fundamental phenomenon of

CNT/polymer nanocomposites, atomistic simulation can help to investigate the behavior of materials at the nanometer scale.

The molecular dynamics (MD) simulation has been developed as an important tool for analyzing and understanding material behavior at the atomic scale, and may lead to new and exciting theoretical and experimental insights. The MD simulation is essentially the numerical solution of Newton's equations of motion for an ensemble of atoms with interacting potentials. The MD simulation process consists of three parts: (1) a set of initial conditions (for example, initial positions and velocities of all atoms in the system); (2) the interaction potentials representing the forces between all the atoms; (3) the evolution of the system in time by numerical integration of the equation of motion for all of the atoms in the system. Using the algorithm above, MD simulation can be performed for several different ensembles, such as microcanonical (NVE), canonical (NVT) and isothermal-isobaric (NPT). The temperature and pressure can be held constant by adding an appropriate thermostat and barostat. Applying MD simulation to CNT/polymer composites allows for an investigation into the effect of SWCNTs on polymer structure and the interfacial interaction between the SWCNTs and polymer matrix.

1.2 Literature Review

Because of their exceptional mechanical properties, CNTs have been extensively utilized as reinforcements in composite materials [3, 4]. The CNTs have nanoscale dimensions but the polymer itself is often regarded in composites as a bulk matrix material, making it a challenge to properly characterize the properties of the CNT/polymer hybrids using conventional continuum theory. Over the past decade, the mechanical properties of CNT-reinforced nanocomposites have been modeled by many researchers using MD simulation [5-7], continuum mechanics [8-10], and multi-scale simulation [11, 12].

Han and Elliott [5] investigated the mechanical properties of nanocomposites with

various volume fractions of (10, 10) SWCNTs embedded in an amorphous polymer matrix. Results indicated that when the interaction between the CNTs and polymer is strong, the interfacial effect cannot be ignored in the material modeling. The elastic moduli for the SWCNTs/polyethylene nanocomposites were predicted by Griebel and Hamaekers [6] using MD simulation. The simulation predicted that for nanocomposites with very long CNTs, the longitudinal modulus demonstrated excellent agreement with the predictions of the micromechanical rule of mixtures. Zhu et al. [7] performed MD simulation on a SWCNT-reinforced Epon 862 matrix, and showed that long CNTs can significantly improve the modulus of the nanocomposites. According to the results in the literature [6, 7], the atomistic interaction between the CNTs and polymer appears to have no significant effect on the longitudinal modulus of the nanocomposites if it is reinforced by the long CNTs. Moreover, the moduli of the nanocomposites can be properly modeled using the continuum micromechanics model (rule of mixtures). Liu and Chen [8] proposed a representative volume element based on continuum mechanics to evaluate the effective mechanical properties of CNT nanocomposites. The finite element analysis revealed that the load carrying capacities of CNTs in a matrix are significant. Luo et al. [9] investigated the effects of CNT spatial distribution and geometry on the modulus of CNT nanocomposites using finite element analysis. The results illustrated that the effects due to fiber volume fraction and aspect ratio are similar to those of conventional short-fiber composites, because the interfacial effects were not considered in the continuum mechanics modeling, some essential characteristics of atomistic/nanoscales may be disregarded in the continuum analysis [8, 9]. Selmi et al. [10] presented a comparative study of the continuum micromechanical models employed to predict the elastic properties of single-walled nanocomposites. Hammerand et al. [11] conducted a micromechanical analysis of the CNT nanocomposites by introducing an interphase layer between the CNTs and the matrix to simulate the imperfect load transfer or imperfect bonding. The dimension of the interphase was determined by requiring that it had the same volume

fraction as the CNTs. Gates et al. [12] provided details of this current multi-scale modeling and simulation approach, and applied it to advanced materials such as nanotube-reinforced polymer composites for structural applications. Among the aforementioned approaches, it has been found that the longitudinal properties of the CNTs composites are mostly of concern whereas the investigations on the transverse properties are relatively few. In addition, the effects of atomic interactions between the CNTs and the surrounding polymer, which may play an important role in the mechanical responses of the nanostructured materials, are rarely explored and considered in the material modeling.

Although SWCNTs have exceptionally high axial strengths and axial Young's moduli, a few results [13] indicated that the SWCNT reinforced nanocomposites cannot fully produce the impressive mechanical characteristics possessed by their nanoscale constituents. Mokashi et al. [14] further indicated that if the load cannot be effectively transferred from the matrix to the CNTs, Young's modulus and tensile strength of the nanocomposites can be less than that of pure resin. The mechanical performance of the nanocomposites appears to rely heavily on the load transfer efficiency from the surrounding matrix to the CNTs, and therefore understanding the stress distribution of the CNT embedded within the nanocomposites has become an essential issue, especially for nanoscale reinforcement.

In conventional composites, the load transfer efficiency as well the interfacial shear strength (ISS) between the fiber and composites is determined based on fragmentation tests [15-17] and fiber pull-out tests [17-19]. For nanocomposites, due to the nano/submicron scale of the reinforcement, experimentally measuring the interfacial strength of nanocomposites is difficult [20, 21]. Instead, numerical simulations based on the concept of fiber pull-out have been extensively employed to evaluate the interfacial strength of nanocomposites [22-26]. Gou et al. [22] examined the ISS of CNTs/epoxy nanocomposites using MD simulation, and revealed an ISS of around 75 MPa. Lordi and Yao [23] studied the binding energy and sliding frictional stresses between pristine CNTs and various matrix polymers. The results indicated

4

that polymers with hydroxy and phenyl side-groups exhibit strong interfacial adhesion. In addition, helical polymer conformation is essential to the strength of the interface. Frankland et al. [24] investigated the effects of chemical cross-linking across the CNT/polymer interface on the shear strength and the critical length required for load transfer. A relatively low density of chemical bonds in the interface was shown to provide an order of magnitude improvement in the shear strength of CNT/polymer interface and the corresponding critical length decreased. Likewise, the establishment of cross-links between the SWCNTs and polymer is an effective way to increase the interfacial shear strength of nanocomposites as demonstrated by Chowdhury and Okabe [25]. Zheng et al. [26] examined the influences of sidewall modification of the SWCNTs with various functional groups on the interfacial bonding. Results showed that for low densities of functionalized carbon atoms, the interfacial bonding, and shear stress between the CNTs and polymer matrix was drastically increased. In addition to the molecular simulation, a hierarchical multi-scale model was proposed by Namilae and Chandra [21] to study the interfacial mechanics in CNT reinforced nanocomposites. An interfacial strength as high as 5 GPa can be achieved by chemically bonding the CNTs and matrix. Based on the continuum mechanics approach, Li and Chou [27] simulated the load transfer in CNT reinforced nanocomposites for both van der Waals (vdW) interface and prefect bonding. The shear stress and normal stress in the CNTs with a perfect interface were shown to be much larger than with a vdW interface.

The research suggests that when covalent bonded cross-links between the CNTs and surrounding polymer are established, the ISS of the interface can be dramatically modified. Because most results were generated using the fiber pullout simulation, only the ISS between the CNTs and polymer has been presented and no constructive correlation between the ISS and the mechanical properties of the nanocomposites has been established. In fact, the mechanical behavior of nanocomposites, such as the tensile Young's modulus, mainly depends on the efficiency of the load transfer from the surrounding matrix to the

nano-reinforcement. In other words, the level of stress carried by the CNTs influences the mechanical responses of the nanocomposites. If the loading applied to the nanocomposites cannot be effectively transferred to the CNTs, the efficiency of the reinforcement could be dramatically decreased.

1.3 Research Motivation and Approach

In this study, the research methodology is divided into three sections. The first section establishes an equivalent solid cylinder with appropriate mechanical properties to take the place of the atomistic structures of SWCNTs in the SWCNT reinforced nanocomposites. The second section models the extent of atomistic interaction between the SWCNTs atoms and the surrounding polyimide polymer by an effective interphase so that the information of the atomic scale interphase is considered in the continuum media. The continuum micromechanical model characterizes the mechanical properties of SWCNT/polyimide nanocomposites and the results are compared with those obtained directly from the MD simulations. The final section characterizes the load transfer efficiency of the SWCNTs subjected to axial loading using MD simulation. The local stress distribution of the CNTs is then obtained using the Lutsko stress formulation [28, 29], and the derivative of potential function from which the load transfer efficiency in the CNTs was determined. In addition, the effects of the atomistic interactions between the CNTs and the surrounding polyimide on the load transfer efficiency of CNTs are explored. The correlations between the tensile moduli of nanocomposites and the load transfer efficiency in terms of the different interfacial adhesions are also discussed.

CHAPTER 2   DETERMINATIONS OF THE EQUIVALENT PROPERTIES OF SOLID CYLINDER FOR SWCNTS

2.1 Generation of SWCNTs Molecular Structures and Equivalent Solid Cylinder

The configuration of SWCNTs is a hollow, cylindrical structure that consists of hexagonal carbon rings. As reinforcements in composite materials, the fundamental mechanical properties of the SWCNTs are defined in the conventional manner so that the existing micromechanical model can be directly implemented into the CNT nanocomposites [30, 31]. In general, reinforcements in the mechanics of composites are regarded as solids with homogeneous material properties. The original attributes of the cylindrical hollow structure of SWCNTs can evidently not satisfy the stated requirement; an equivalent solid cylinder is necessary to properly interpret the mechanical properties of the atomistic SWCNT structure in the continuum solid model and transform accurately into the SWCNTs nanocomposites. The equivalent solid cylinder is assumed to have the same geometric configuration as that of the original CNTs-structures. The radius of the equivalent solid cylinder is equal to the distance from the center of a CNT to the circumferential atoms, as shown in Fig. 2-1. In this study, only zig-zag type SWCNTs, (10,0), (14,0), and (18,0), with respective radii of, 3.9, 5.5, and 7.1Å, were selected for the demonstration, but the approach presented hereafter is not limited to these cases. In addition, the zig-zag type SWCNTs of length 85.2 Å were constructed by repeating the unit cell several times along its axial direction (1 direction) as shown in Fig. 2-2.

2.1.1 Interatomistic potential for SWCNTs

The fundamental mechanical properties of SWCNTs were characterized using MD simulation, in which the molecular structure of SWCNTs as well as the atomistic interaction were appropriately constructed and specified. In the MD simulation, two kinds of atomistic

interactions were considered in the modeling of SWCNTs; one is bonded interaction, such as the covalent bonding, and the other is the non-bonded interaction, namely van der Waals and electrostatic forces. For the SWCNTs, the primary structure was constructed by bonded atomistic interaction between the carbon atoms. Such bonded interaction is described by the potential energy that consists of bond stretching, bond angle bending, torsion, and inversion, as illustrated in Fig. 2-3 [32]. The explicit form of the total potential energy for bonded interaction is expressed as

$$U_{CNT} = \sum U_r + \sum U_\theta + \sum U_\phi + \sum U_\omega \tag{2.1}$$

where U_r is the bond stretching potential; U_θ is the bond angle bending potential; U_ϕ is the dihedral angle torsional potential; and U_ω is the inversion potential. For small deformations, the stretching and bending behavior can be modeled using elastic springs and the corresponding potentials are approximated as [33]

$$U_r = \frac{1}{2} k_r (r - r_0)^2 \tag{2.2}$$

$$U_\theta = \frac{1}{2} k_\theta (\theta - \theta_0)^2 \tag{2.3}$$

For the dihedral torsional potential and inversion potential, Li and Chou [33] adopted a simplest harmonic form to incorporate the two interactions into a single equivalent term as

$$U_\tau = U_\phi + U_\omega = \frac{1}{2} k_\tau (\phi - \phi_0)^2 \tag{2.4}$$

In Eqs. (2.2)-(2.4), k_r, k_θ and k_τ are the bond stretching force constant, angle bending

force constant and torsional resistance, respectively. The constants $k_r = 93800 \dfrac{Kcal}{mole \cdot nm^2}$

and $k_\theta = 126 \dfrac{Kcal}{mole \cdot rad^2}$ selected from AMBER force field for carbon-carbon

atomic-interaction [34] were employed in our molecular simulation. On the other hand, for the

force constant k_τ, since Li and Chou [33] indicated that this value may not have significant

influence on CNT Young's modulus, the constant $k_\tau = 40 \dfrac{Kcal}{mole \cdot rad^2}$ was borrowed directly

from their work. The parameters r_0, θ_0 and ϕ_0 represent bond length, bond angle and

dihedral torsional angle in the equilibrium position in the CNT atomistic structures, which are

equal to 1.42 nm, 120° and 180°, respectively. The DL-POLY package originally developed by

Daresbury Laboratory [35] was employed in our MD simulation, for which the Dreiding

potential [36] was utilized to model the inter-atomic potential of carbon-carbon bonding. For

the bond stretching and angle bending behavior, the mathematical forms in the Dreiding

potential are exactly the same as those given in Eqs. (2.2) and (2.3). For the dihedral torsion

and inversion, the Dreiding torsional potential accounting for these two components is

expressed as

$$U_\tau = U_\phi + U_\omega = A[1 - \cos(m(\phi - \phi_0))] \tag{2.5}$$

Because the carbon–carbon bonding in the hexagonal graphite is in resonance, the parameter

m in Eq. (2.5) should be equal to 2 [36]. In addition, the parameter A is chosen according to

the assumption that the Dreiding torsional potential should correspond to the dihedral

torsional potential given in Eq. (2.4). When A is equal to 10.02kcal/mole, the Dreiding

torsional potential was found to be in good agreement with the torsional potential and a

comparison of torsional potential (Eq. (2.4)) and the Dreiding torsional potential (Eq. (2.5)) is

shown in Fig. 2-4. For this reason, values of m = 2 and A = 10.02 kcal/mole were used in Eq.

(2.5) for the Dreiding torsional potential.

2.1.2 Effect of van der Waals interaction on the properties of atomistic SWCNTs

The non-bonded atomistic interaction between the carbon atoms is generally referred to as the van der Waals force. Many researches consider the van der Waals force as normally having only a negligible influence on the overall mechanical behavior among the atomic interactions of the SWCNTs. [33, 37]. Agrawal et al. [38] investigated Young's modulus for SWCNTs under various conditions using MD simulation. Results indicated that the van der Waals interaction increases the value of axial Young's modulus by about 1%. However, Chen et al. [39] performed MD simulation on SWCNTs showing that the effect of van der Waals force increased the axial Young's modulus and shear modulus of SWCNTs by up to 9% and 12%, respectively. However, no definite conclusions have been drawn. This section investigates the effect of van der Waals interactions on SWCNTs.

The van der Waals force can be characterized using the Lennard-Jones (L-J) potential as

$$U_{vdW} = 4u \left[\left(\frac{r_0}{r_{ij}} \right)^{12} - \left(\frac{r_0}{r_{ij}} \right)^6 \right] \tag{2.6}$$

where r_{ij} is the distance between the non-bonded pair of atoms. For the hexagonal graphite, the parameters value $u = 0.0556$ kcal/mole and $r_0 = 3.40$ Å, which were suggested in the literature [40], were adopted in the modeling. To evaluate the axial Young's modulus of the SWCNTs, the potential energy of the SWCNTs in the initial state (stress-free state) was calculated through MD simulation. A small axial elongation was then applied to one end of the SWCNTs with the other end fixed. After an energy minimization process, the energy in the deformation configuration was evaluated again through the MD simulation. Based on linear elasticity theory, the Young's moduli are derived from the strain energy variation with respect to the strain increment as

$$Y = \frac{2\Delta U}{\varepsilon^2 V_{CNT}} \qquad\qquad (2.7)$$

$$V_{CNT} = \pi \left[\left(r_0 + \frac{t}{2} \right)^2 - \left(r_0 - \frac{t}{2} \right)^2 \right] L_0 \qquad\qquad (2.8)$$

where Y is the axial Young's modulus of SWCNTs, ΔU is the strain energy variation, ε is the strain increment, L_0 is the length of SWCNTs, V_{CNT} is the volume of the SWCNTs, r_0 is the radius and t is the assumed tube wall thickness equal to 0.34 nm [39]. The effects of van der Waals force on axial Young's modulus of the SWCNTs with three different sizes are illustrated in Table 2-1. Results indicate the axial Young's moduli of SWCNTs appear to not depend on the van der Waals force consideration and it is in good agreement with the experimental value [AA,41]. The van der Waals force on SWCNTs is considered in this research.
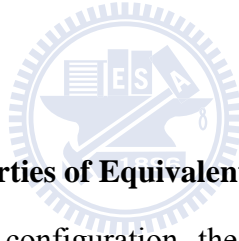
2.2 Determination of the Properties of Equivalent Solid Cylinder

In addition to the geometric configuration, the associated mechanical properties of the equivalent solid cylinder have to be determined accurately in accordance with the atomistic structures of SWCNTs. Because of the geometric configuration of the SWCNTs, the corresponding properties of the equivalent solid cylinder are assumed to be transversely isotropic. The five independent material constants in the effective solid need to be evaluated. To accomplish this objective, the discrete atomistic structures of SWCNTs with energy minimization were initially constructed using MD simulation. By applying a desired displacement on the SWCNTs, the strain energy variation was calculated in terms of the deformation. Meanwhile, the same deformation was applied to the equivalent solid. According to the hypothesis that the strain energy variations in the SWCNTs atomistic structure and the equivalent solid continuum should be the same for the same deformation, the corresponding material constants in the equivalent solid were evaluated.

2.2.1 Young's modulus E_1

To evaluate the properties of the equivalent solid cylinder, the deformation that followed the previous process was applied to the SWCNTs and the potential energy variation between the initial and deformed configuration in the SWCNT's atomistic structures associated with axial strain increment was deduced. The simulation process is illustrated in Fig. 2-5. When a continuum solid is subjected to simple tension, based on linear elasticity theory, the Young's moduli can be derived from the strain energy variation with respect to the strain increment

$$E_1 = \frac{2\Delta U}{\varepsilon^2 V_{solid}} \tag{2.9}$$

$$V_{solid} = \pi r_0{}^2 L_0 \tag{2.10}$$

where ΔU is the strain energy variation, ε is the strain increment, L_0 is the length of SWCNTs, and V_{Solid} is the volume of the continuum solid. The Poisson effect was not considered in the above derivation. The potential energy variation obtained from the MD simulation was regarded as the energy difference in the equivalent solid for the same axial deformation. Using Eq. (2.9), the longitudinal moduli of the solid cylinder with three different radii were evaluated, and the results are presented in Table 2-2. The Young's modulus of the equivalent solid cylinder was observed to decrease as the cylinder radii increase. The trend matches that trend presented in [30]. The Young's modulus of the equivalent solid cylinder is slightly higher than that obtained in [30] for the same zig-zag type tubes. This discrepancy may be due to the different definitions of the cross sectional area as well as the force potentials used in modeling the atomistic interaction of the carbon atoms. A critical review on the effective Young's moduli of SWCNTs has been presented in the literature [31, 42].

2.2.2 Shear modulus G_{12}

For the calculation of the shear modulus of the equivalent solid, the atomistic structure of

SWCNTs was subjected to a torsional displacement ϕ at one end together with the fixed boundary condition at the other end as shown in Fig. 2-6. Similar boundary conditions were also adopted in the literature for the evaluation of the shear modulus of SWCNTs [43]. After the energy minimization process, the energy difference (ΔU) of the deformed SWCNTs with respect to the torsional angle ϕ was calculated through MD simulation. If the deformation is very small and within the linear range, the associated shear modulus of the equivalent solid cylinder in terms of the torsional angle and energy variation is given as [44]

$$G_{12} = \frac{2\Delta U}{\phi^2 J_{solid}} L_0 \qquad (2.11)$$

$$J_{solid} = \pi r_0^{\,4} \qquad (2.12)$$

where J_{Solid} is the cross-sectional polar inertia of the equivalent solid cylinder, and L_0 is the length of the SWCNTs. The shear moduli calculated in Eq. (2.11) for the equivalent solids are also shown in Table 2-2. Analogous to the longitudinal modulus, the shear modulus declines as the CNT radius increases.

2.2.3 Poisson's ratio ν_{12}

In addition to the Young's modulus and shear modulus, the determination of Poisson's ratio of the equivalent solid was directly motivated by the continuum mechanics concept. Instead of displacement constraints imposed on the boundaries, axial stress was applied to both ends of CNTs to diminish the end constraint effect. In the MD simulation, a modified NPT ensemble with the characteristics of varying simulation box in shape and size [45] was employed such that uniaxial stress can be independently applied to both ends of the SWCNTs with stress free in the lateral direction. Again after the energy minimization process, the equilibrated CNT atomistic structure was obtained, and Poisson's ratio was defined as

$$\nu_{12} = -\frac{\varepsilon_r}{\varepsilon} \qquad\qquad (2.13)$$

where ε_r is the lateral strain in a nanotube and is defined as $(r - r_0) / r$ where r_0 and r are the SWCNTs radii before and after the stress is applied, respectively, and ε represents the axial strain. The Poisson's ratio obtained based on Eq. (2.13) for the zig-zag type SWCNTs with various radii are presented in Table 2-2. Poisson's ratio for the equivalent solid cylinder appears to not be sensitive to the SWCNT radius.

2.2.4 Young's modulus E_2 and Poisson's ratio ν_{23}

Because of the characteristics of the atomistic structures of the SWCNTs, the mechanical properties in the lateral direction (in-plane properties) are isotropic; thus, only two material constants are independent and need to be determined. Young's modulus E_2 and Poisson's ratio ν_{23} in the transverse direction were selected for the following evaluation.

Radial displacement was applied to the atoms located at the circumference of the SWCNTs atomistic structures as shown in Fig. 2-7, and the energy variation of the SWCNTs after the deformation was calculated using the MD simulation. In a similar manner, the same radial displacement was applied to the equivalent solid, and the energy variation was calculated using finite element analysis. By adjusting the values of E_2 and ν_{23} in the equivalent solid cylinder such that the energy variation in the equivalent solid was equal to that obtained from SWCNTs atomistic structure, the transverse properties in the effective solid were determined accordingly.

In the equivalent solid, the energy variation was calculated using a commercial finite element program ANSYS with a 2-D plane element. Because only one equation (energy equivalence equation) is available, it is unfeasible to yield a unique solution for the two unknowns, E_2 and ν_{23}, and thus multiple solutions are always generated in the above calculation. To understand the sensitivity of the E_2 and ν_{23} values to the mechanical responses

of SWCNT-reinforced nanocomposites, we set ν_{23} to 0.2 and 0.4, respectively, and calculated the corresponding values of E_2 in the equivalent solids. The values of ν_{23} and the corresponding values of E_2 for three different CNT radii are shown in Table 2-3. The two different groups of E_2 and ν_{23} together with other material constants, E_1, G_{12}, and ν_{12}, which are shown in Table 2-4, were entered into the Mori-Tanaka micromechanical model [46] for characterizing the properties of the SWCNT nanocomposites. The Young's modulus, shear modulus and Poisson's ratio of polymer matrix were assumed to be equal to 3.67 GPa, 1.41 GPa and 0.3, respectively. In addition, assuming a volume fraction of SWCNTs equal to 0.08, the mechanical properties of SWCNT nanocomposites were calculated based on Mori-Tanaka micromechanical model and are shown in Table 2-5. Comparing the moduli of the SWCNT nanocomposites based on the two different properties of equivalent solids reveals that the mechanical properties of the SWCNTs composites are not dramatically affected by the transverse properties of the effective cylindrical solids. Therefore, we hereafter adopted ν_{23} as 0.2 for the equivalent cylindrical solid and then calculated the related Young's modulus E_2. All the mechanical properties of the equivalent cylindrical solid, calculated based on the energy equivalence concept, are summarized in Table 2-2.

CHAPTER 3   EFFECTIVE INTERPHASE MODEL FOR SWCNTS/POLYIMIDE NANOCOMPOSITES

When the hollow molecular structure of SWCNTs was converted into a solid cylinder through the concept of energy equivalence as presented in the early section, the mechanical behavior of SWCNT nanocomposites can be predicted using the conventional two-phase micromechanical model [46]. In the two-phase model, the reinforcements are always assumed to be perfectly bonded with the surrounding polymer matrix. However, in SWCNT reinforced nanocomposites, the interfacial bonding is not perfect, and is dominated by the non-bonded interaction consisting of electrostatic and van der Waals interactions. Moreover, the extent of atomistic interaction between the SWCNTs and surrounding matrix may influence the mechanical responses of the nanocomposites. As a result, a continuum micromechanical model being able to account for the inter-atomic effect in the modeling of SWCNT nanocomposites is indispensable. In this section, the atomistic interaction between the SWCNTs and the polyimide matrix is characterized by the effective interphase, the corresponding properties of which were determined from the molecular interaction energy calculated from the MD simulation. By knowing the properties of the effective interphase in conjunction with the equivalent solid cylinder of SWCNTs, the SWCNT nanocomposites that were originally discrete atomistic structures can be interpreted using a three-phase continuum micromechanical model as demonstrated in Fig. 3-1.

3.1 Construction of SWCNTs/Polyimide Nanocomposites

In order to understand the atomistic interaction between the SWCNTs and the surrounding polyimide polymer, the molecular structure of SWCNTs/polyimide nanocomposites employed in the MD simulation were constructed initially. A simulation unit with periodic boundary conditions that contain SWCNTs embedded in the amorphous polyimide molecular chains was constructed and is shown in Fig. 3-1(a). The polyimide

polymer is generated by 10 repeated monomer units, and the corresponding chain number is dependent on the size of the simulation box. Fig. 3-2 illustrates the polyimide monomer unit. For the potential of polyimide polymers, the Dreiding force field [36] was employed to describe the covalent bonding as well as the non-bonding interaction in the polyimide polymer. In the Dreiding force field, the non-bonded interaction was depicted by the L-J potential between two different kinds of atoms, for which the parameters were derived from the Lorentz Berthelot combining rule [47]. Moreover, the atomistic interaction between polyimide molecular and SWCNTs were directly modeled using the Dreiding force field although the modified parameters in the Dreiding force field were employed to model the SWCNTs, as discussed earlier. Different SWCNT radii of 3.9, 5.5, and 7.1 Å were considered as reinforcements in the nanocomposites, and the corresponding numbers of polyimide chains was equal to 8, 16, and 26, respectively. Although the three different radii were utilized in these SWCNTs/polyimide molecular structures, the volume fractions of SWCNTs in the nanocomposites remain the same. The MD simulations for the SWCNTs/polyimide nanocomposites were conducted using a DL-POLY package [35]. The equilibrated molecular structure with a minimized energy was achieved by sequentially performing MD simulations of the NVT and NPT ensembles. The NVT ensemble has a fixed volume and temperature during the simulation, and the NPT ensemble has a fixed pressure and temperature. The purpose of the NVT ensemble simulation conducted at 1000 K for 200 ps was to supply enough kinetic energy to the polyimide molecules so that a homogeneous molecular structure within the simulation box can be achieved. During the process, the SWCNT atoms were frozen, meaning that the carbon atoms in SWCNTs were fixed at their original position throughout the whole simulation [48]. The NPT process was then set to 0 atm so that the simulation box could have traction-free boundary conditions. Three sub-steps were introduced for the temperature drop from 1000 to 0 K in the NPT process. In the first and second steps, the temperature was set at 600 K and 300K respectively, and the simulation time for each step

was 200 ps with a time increment of 1 fs. In the third stage, the modified NPT ensemble that could vary shape and size of the simulation box [45] was conducted to construct the molecular system with a stress-free state. The entire system was equilibrated at 0 K under stress-free conditions for another 150 ps. The frozen atoms of SWCNTs were released as the last step so that the entire nanocomposites system could be equilibrated at the stress-free state.   During the simulation, the total potential energy variation was examined, and after the quantity fluctuated around a certain mean value for a while, the system was considered to be in equilibrium. Figs. 3-3 and 3-4 demonstrate the potential energy history of the nanocomposites as well as the temperature variation during the third step in the modified NPT ensemble, respectively. The potential energy appears to reach a stable level after 10 ps, and the temperature approaches 0 K. Based on the observations, the current molecular structure is assumed to be in the equilibrium condition and suitable for characterizing molecular structure as well as the material properties. The volume fractions for the three different sizes of SWCNT radius 3.9, 5.5, and 7.1 Å were 6.28, 6.43, and 6.67 %, respectively.

In addition to SWCNTs/polyimide nanocomposites, the molecular structure of polyimide, which has 8 polyimide chains, was also constructed to obtain the mechanical property of the matrix in the three-phase continuum micromechanical model in the following section. Fig. 3-5 shows the equilibrium molecular structure of polyimide polymer. Similar to the SWCNTs/polyimide nanocomposites, the equilibrium molecular structure of polymer was also constructed using the previous simulation processes.

3.2 Characterization Atomistic Structure of the Nanocomposites
3.2.1 Density distribution

The density distribution of polyimide polymer near the CNTs was calculated from the atomistic morphology of the nanocomposites derived from the MD simulation. The cross section of SWCNTs/polyimide nanocomposites is illustrated in Fig. 3-6 and the density

distribution of polyimide was evaluated according to the following formula

$$\rho(r) = \frac{g_r}{V_r} \tag{3.1}$$

where $V_r = \pi((r+dr)^2 - r^2)L_0$ indicates the volume of a cylindrical shell near the CNTs with length equal to L_0, and g_r denotes the total atom mass within V_r. The density distributions of the SWCNTs and the polyimide polymer in the radial direction for the three different CNT radii are illustrated in Fig. 3-7. In the region near the SWCNTs, the polyimide density is seen to be relatively high and then declines to a normal value (1.31 g/cc) [49] when far from the SWCNTs.

In addition, the order parameter distribution S could be calculated for deeply understanding the morphology of polyimide molecular surrounding the SWCNTs. The order parameter was defined as [50]

$$S(r) = \left\langle 3\cos^2\theta - 1 \right\rangle / 2 \tag{3.2}$$

where θ is the angle between the sub vector and the reference vector, $\langle \ \rangle$ denoted the average over the sub vectors in the cylindrical shell as shown in Fig. 3-7. The sub vector in the polyimide polymer may be defined as shown in Fig. 3-8 and the corresponding reference vector is defined from the center of SWCNTs to the middle of the sub vector. The limiting values of S are 1, 0 and -0.5 for perfectly parallel, random vectors, and vectors perpendicular to the surface of SWCNTs, respectively. The order parameter distribution of the polyimide polymer in the radial direction for the three different CNT radii is also illustrated in Fig. 3-7. In the region near the SWCNTs, the polyimide polymer appears to almost lie on the SWCNTs.

Almost all of the high density of polyimide regions was lay next to the SWCNTs. It indicated that due to the interfacial interaction between the SWCNTs and polymer matrix, the SWCNTs attracted the surrounding polyimide polymer onto the surface. As a result, the density of polyimide polymer in the region near the SWCNTs is higher than in other regions.

3.2.2 Non-bond gap

From Fig. 3-7, a clear gap with very low molecular density exists between the SWCNTs and the surrounding polyimide matrix. In this study, the gap is referred to as the non-bonded gap because it is caused by the non-bonded force field between the SWCNTs and the polymeric matrix. To qualitatively characterize the dimension of the non-bonded gap, a radial volume element is proposed, as shown in Fig. 3-9, where $\Delta\theta$ is the angle between two radial lines emitted from the center of the SWCNTs, and Δz is the length in the SWCNTs longitudinal direction. For each incremental rotation (10°) of the volume element with respect to the z-axis, the positions of SWCNT and polyimide atoms within the element were counted. The maximum radial distance for the SWCNT atoms within the volume element is denoted as r_{CNTs}^{max}, and the minimum radial distance for the polyimide atoms is represented as r_{PI}^{min}. The non-bonded gap between the SWCNTs and the polyimide matrix within the unit volume is introduced as

$$r_{non-bond} = r_{PI}^{min} - r_{CNTs}^{max} \qquad (3.3)$$

Fig. 3-10 illustrates the measurements of the maximum radial distance for SWCNT atoms together with the minimum radial distance for polyimide atoms for each rotational increment. When the radial volume element rotates around 360°, the average value of the $r_{non-bond}$ is regarded as the non-bonded gap of the nanocomposites. Table 3-1 indicates the non-bonded gap calculated from the nanocomposites with three different SWCNT radii. The non-bonded

gap decreases slightly as the SWCNT radius increases. Nevertheless, the dependence of the non-bonded gap on the SWCNT radius was insignificant.

3.2.3 Non-bond energy

In addition to the non-bonded gap, the non-bonded energy between the SWCNTs and the polyimide matrix was estimated from the MD simulation. When calculating the non-bonded interaction, only the van der Waals interaction modeled by the Lennard–Jones potential function was considered. In reality, some kind of cross-linking between the SWCNTs and polyimide matrix may be occurring in the curing process. This phenomenon has not been included in the present model. The total non-bonded energy within the nanocomposites comprises not only the interaction between the SWCNTs and the polyimide, but also the SWCNTs and the polyimide molecular chains. Therefore, the non-bonded energy between the SWCNTs and polyimide is calculated by subtracting the non-bonded energy of the SWCNTs and polyimide polymer from the total non-bonded energy and this can be expressed as

$$U_{PI-CNTs} = U_{Total} - U_{CNTs} - U_{PI} \qquad (3.4)$$

where U_{total} is the total non-bonded energy obtained from the nanocomposites. U_{CNTs} and U_{PI} are the non-bonded energies of the SWCNTs and the polyimide molecular chain, respectively. The non-bonded energy of the polyimide molecular chain was evaluated in the simulation box where the SWCNTs were removed, and only the molecular structures of the polyimide matrix remained. In a similar manner, the non-bonded energy of SWCNTs was calculated. Using Eq. (3.4), the non-bonded energy between the SWCNTs and the polyimide was determined. The non-bonded energy provides a relative indication of the extent of interaction between the SWCNTs and the surrounding matrix. If the non-bond interaction can be further employed to represent the properties of an equivalent interphase with a dimension equal to the non-bond

gap, the mechanical properties of the nanocomposites may be described by the three-phase micromechanical model comprising the SWCNTs, effective interphase, and polyimide polymer.

To achieve this goal, the degree of interaction between the SWCNTs and the matrix is characterized in terms of the normalized non-bonded energy, which is defined as the non-bonded energy divided by the surface area of the SWCNTs. The normalized non-bonded energy was assumed to be associated with the non-bonded gap in the form of

$$U(r) = \frac{1}{6} kr^6 \qquad (3.5)$$

where r is the non-bonded gap, and k is the parameter to be determined. Based on the normalized non-bonded energy, the corresponding normalized interaction force was obtained by differentiating the energy with respect to the distance such that

$$F(r) = -\frac{\partial U}{\partial r} = -kr^5 \qquad (3.6)$$

The negative sign for the force in Eq. (3.6) represents the attractive interaction. Eqns. (3.5) and (3.6) can also be interpreted as the strain energy of a unit element with length equal to the non-bond gap, r, with a cross-sectional area equal to 1, when it is subjected to the applied loading kr^5. According to 1D elasticity, the strain energy of the unit element is represented as

$$U = \frac{\sigma^2}{2E} r \qquad (3.7)$$

where E is the Young's modulus of the equivalent unit element, and σ is equal to kr^5, which

is the loading applied to the unit area (so-called stress). From the hypothesis that the strain energy of the unit element is equivalent to the normalized energy given in Eq. (3.5), the modulus of the equivalent unit element is given as

$$E = 3kr^5 = \frac{18U(r)}{r} \tag{3.8}$$

In the above calculation, only the strain energy caused by axial loading was adopted to illustrate the normalized non-bonded energy of the nanocomposites obtained from the MD simulation. Once the non-bonded gap and the normalized non-bonded energy was calculated, the elastic moduli of the equivalent interphase can be determined using Eq. (3.8). Table 3-1 demonstrates the normalized non-bonded energy of the nanocomposites calculated for the different CNTs radii. As the radius increases, the corresponding normalized non-bonded energy decreases, indicating a reduction in interaction strength.

3.3 Elastic Constants of Molecular Structures

The mechanical properties of the equilibrated molecular configuration of SWCNT nanocomposites were also predicted using MD simulation. To achieve this purpose, small strains were applied to the system along each direction. The application of a tensile strain equal to 0.0005 was accomplished by uniformly expanding the dimensions of the system in the direction of the deformation and re-scaling the new coordinates of the atoms to fit within the new dimensions. After this initial deformation, the atoms were allowed to equilibrate within the new system dimensions for 100 ps at 0K in the NVT process. Once the equilibrium condition was accomplished in the deformed state, the associated stress was calculated from the virial theorem and the stiffness matrix C_{ijkl} of the nanocomposites was measured as the derivative of the stress associated with the corresponding strain component

$$C_{ijkl} = \frac{\Delta\sigma_{ij}}{\Delta\varepsilon_{kl}} \tag{3.9}$$

where the stress was calculated from the virial theorem [47] and was expressed as

$$\sigma_{ij} = -\frac{1}{V^{Total}}\left(\sum_{i<j} r_{ij}f_{ij}^{T}\right) \tag{3.10}$$

In Eq. (3.10), r_{ij} and f_{ij} denote the atomic distance and the corresponding interaction force between any two atoms within the cut-off distance. V^{Total} represents the total volume of the system. As shown in Eq. (3.10), the model was simulated at 0 K, so the temperature effect was neglected in the stress computation. Due to the assumption that SWCNTs/polyimide nanocomposites have orthotropic symmetry, the stress-strain relation could be reduced to

$$\begin{Bmatrix} \sigma_{11} \\ \sigma_{22} \\ \sigma_{33} \end{Bmatrix} = \begin{bmatrix} C_{11} & C_{12} & C_{13} \\ C_{21} & C_{22} & C_{23} \\ C_{31} & C_{32} & C_{33} \end{bmatrix} \begin{Bmatrix} \varepsilon_{11} \\ \varepsilon_{22} \\ \varepsilon_{33} \end{Bmatrix} \tag{3.11}$$

where $C_{12} = C_{21}$, $C_{13} = C_{31}$ and $C_{23} = C_{32}$. Hence, only five independent elastic constants exist in the stiffness matrix. However, in the molecular simulation, constructing such a homogeneous molecular structure that the values of C_{12} and C_{21}, C_{13} and C_{31}, and C_{23} and C_{32} in the stiffness matrix are each the same is difficult. The values of elements in the stiffness matrix of the SWCNTs/polyimide nanocomposites for the three different CNT radii are shown in Table 3-2. The variations are quite small (less than 10%), and therefore the current molecular models were believed to be suitable for describing the mechanical properties of the nanocomposites. To calculate Young's modulus for the SWCNTs/polyimide nanocomposites, the stiffness matrix composites can be rewritten as

$$[C] = \begin{bmatrix} C_{11} & \overline{C}_{12} & \overline{C}_{13} \\ \overline{C}_{12} & C_{22} & \overline{C}_{23} \\ \overline{C}_{13} & \overline{C}_{23} & C_{33} \end{bmatrix} \quad (3.12)$$

where $\overline{C}_{12} = \frac{1}{2}(C_{12} + C_{21})$, $\overline{C}_{13} = \frac{1}{2}(C_{13} + C_{31})$ and $\overline{C}_{23} = \frac{1}{2}(C_{23} + C_{32})$. The compliance

matrix of composites S_{ij} was expressed explicitly as [51]

$$[S] = [C]^{-1} = \begin{bmatrix} 1/E_1 & -\nu_{21}/E_2 & -\nu_{31}/E_3 \\ -\nu_{12}/E_1 & 1/E_2 & -\nu_{32}/E_3 \\ -\nu_{13}/E_1 & -\nu_{23}/E_2 & 1/E_3 \end{bmatrix} \quad (3.13)$$

where E and ν indicate the Young's modulus and Poisson's ratio, respectively, and the subscripts denote the direction.

Based on above method, the stiffness matrix of the neat polyimide polymer was derived, and is shown in Table 3-3. Considering that the neat polyimide matrix was an isotropic material and the stiffness matrix was defined as

$$[C] = \begin{bmatrix} \overline{C}_{11} & \overline{C}_{12} & \overline{C}_{12} \\ \overline{C}_{12} & \overline{C}_{11} & \overline{C}_{12} \\ \overline{C}_{12} & \overline{C}_{12} & \overline{C}_{11} \end{bmatrix} \quad (3.14)$$

where $\overline{C}_{11} = \frac{1}{3}(C_{11} + C_{22} + C_{33})$ and $\overline{C}_{12} = \frac{1}{6}(C_{12} + C_{21} + C_{13} + C_{31} + C_{23} + C_{32})$. The compliance

matrix of composites S_{ij} could be expressed explicitly as [51]

$$[S] = [C]^{-1} = \begin{bmatrix} 1/E & -\nu/E & -\nu/E \\ -\nu/E & 1/E & -\nu/E \\ -\nu/E & -\nu/E & 1/E \end{bmatrix} \qquad (3.15)$$

The mechanical properties of polyimide polymer could be determined using Eq. (3.15) as shown in Table 3-4 which is in agreement with experimental value[49], and were then employed in the three-phase micromechanical model.

In this study, based on MD simulation, the moduli of SWCNTs nanocomposites in the longitudinal and transverse directions were estimated, and the results were compared with those derived from the following three-phase micromechanical model.

3.4 Three-Phase Micromechanical Model

Based on the aforementioned derivation, the non-bonded interaction between the SWCNTs and the surrounding polyimide matrix can be appropriately replicated by a continuum-based equivalent interphase. With the mechanical properties of the equivalent solid cylinder (representing SWCNTs), an effective interphase, and polyimide matrix as well as the corresponding geometric parameters, the responses of the SWCNTs nanocomposites can be depicted using the micromechanical model with multiple phases [52, 53]. Notably, three ingredients have been considered in the three-phase model, which is different from the conventional Mori-Tanaka micromechanical model [46] where only two phases were included in the analysis. The explicit formulation of the three-phase model is written as [52]

$$C^* = C^m + \left[(\nu_\Gamma + \nu_\Omega)\{C^\Gamma - C^m\}A_v^{di} + \nu_\Omega\{(C^\Omega - C^\Gamma)A_\Omega^{di}\}\right]\left[\nu_m I + (\nu_\Gamma + \nu_\Omega)\{A_v^{di}\}\right]^{-1} (3.16)$$

where C^* denotes the stiffness matrix for the nanocomposites, C^Ω, C^Γ, and C^m represent the stiffness of the domain of Ω (equivalent solid cylinder), Γ (interphase), and m (polyimide

matrix), respectively, as shown in Fig. 3-1(b); ν_Ω, ν_Γ and indicate the volume fraction of the respective domains. In addition,

$$A_V^{di} = I + E_{Esh}^V \Phi^V \tag{3.17}$$

$$A_\Omega^{di} = I + \Delta E_{Esh} \Phi^\Gamma + E_{Esh}^\Omega \Phi^\Omega \tag{3.18}$$

where

$$\Phi^\Omega = -[(E_{Esh}^V + C^1) + \Delta E_{Esh}(E_{Esh}^\Omega - \frac{\nu_\Omega}{\nu_\Gamma}\Delta E_{Esh} + C^2)^{-1}(E_{Esh}^\Omega - \frac{\nu_\Omega}{\nu_\Gamma}\Delta E_{Esh} + C^1)]^{-1} \tag{3.19}$$

$$\Phi^V = \frac{\nu_\Omega}{\nu_\Omega + \nu_\Gamma}\Phi^\Omega + \frac{\nu_\Gamma}{\nu_\Omega + \nu_\Gamma}\Phi^\Gamma \tag{3.20}$$

$$\Phi^\Gamma = -[\Delta E_{Esh} + (E_{Esh}^\Omega + C^1)(E_{Esh}^\Omega - \frac{\nu_\Omega}{\nu_\Gamma}\Delta E_{Esh} + C^1)^{-1}(E_{Esh}^\Omega - \frac{\nu_\Omega}{\nu_\Gamma}\Delta E_{Esh} + C^2)]^{-1} \tag{3.21}$$

$$\Delta E_{Esh} = E_{Esh}^\Omega - E_{Esh}^V \tag{3.22}$$

$$C^1 = (C^\Omega - C^m)^{-1}C^m \tag{3.23}$$

$$C^2 = (C^\Gamma - C^m)^{-1}C^m \tag{3.24}$$

In the above expression, $V = \Omega + \Gamma$, which is the domain comprising the CNTs and the interphase as well, and E_{Esh}^V and E_{Esh}^Ω indicate the Eshelby's tensor for the domains V and Ω, respectively [54]. It is noted that when the aspect ratio of the inclusion phases are infinite, such as SWCNTs, the Eshelby's tensors can be written explicitly as [55]

$$E_{Esh}^\Omega = E_{Esh}^V = E_{ijkl} \tag{3.25}$$

where

$$E_{1111} = 0 \tag{3.26}$$

$$E_{2222} = E_{3333} = \frac{5 - 4\nu_m}{8(1 - \nu_m)} \tag{3.27}$$

27

$$E_{2233} = E_{3322} = \frac{4v_m - 1}{8(1 - v_m)} \tag{3.28}$$

$$E_{2211} = E_{3311} = \frac{v_m}{2(1 - v_m)} \tag{3.29}$$

$$E_{1122} = E_{2211} = 0 \tag{3.30}$$

$$E_{2323} = \frac{3 - 4v_m}{8(1 - v_m)} \tag{3.31}$$

$$E_{1212} = E_{1313} = \frac{1}{4} \tag{3.32}$$

and v_m is the Poisson's ratio of the surrounding matrix. In this approach, the discrete molecular structure of SWCNT nanocomposites was efficiently converted into a continuum system, and the corresponding properties were simulated using the continuum micromechanical analysis when the equivalent properties were properly determined.

3.5 Results and discussion

Table 3-5 shows the longitudinal moduli of the SWCNTs/polyimide nanocomposites for the three different radii of SWCNTs. As the radius increases, the corresponding modulus of the nanocomposites appears to decrease although the SWCNT volume fractions remains the same. In addition, the moduli of the nanocomposites calculated from the MD simulation are quite close to the conventional micromechanical model (rule of mixture). Therefore, the effect of atomistic interaction between the SWCNTs and polyimide may be neglected in modeling the longitudinal modulus of nanocomposites with continuous SWCNTs as indicated in Refs. [6, 7]. Because of the influence of the effective interphase, the longitudinal modulus of the nanocomposites obtained from the three-phase model is a little higher than that obtained from the MD simulation.

For the transverse moduli of the SWCNTs/polyimide nanocomposites, the results with different radii of SWCNTs are listed in Table 3-6. Similar to the longitudinal moduli, the transverse moduli also decrease as the SWCNT radii increase. Nonetheless, the declining

characteristic observed in the MD simulation and three-phase model was not exhibited in the conventional micromechanical model. Apparently, in the transverse direction, the atomistic interaction effect is more significant, but is not accounted for in the conventional continuum mechanics modeling. In light of the forgone discussion, it is suggested that in the longitudinal direction, the conventional micromechanical model with the equivalent SWCNTs properties is adequate for predicting the moduli of SWCNTs nanocomposites. Alternatively, for the transverse modulus of the nanocomposites, the three-phase model has to be employed to describe the mechanical properties accurately. For the reinforcement efficiency, the SWCNTs with smaller radii have been shown to provide superior mechanical properties in their composites when the volume fractions of SWCNTs remain the same. This suggestion is consistent with the experimental observation that the efficiency of reinforcement varies linearly with the total SWCNT surface area in the nanocomposites [56].

CHAPTER 4   LOAD TRANSFER EFFICIENCY BETWEEN THE SWCNTS AND SURROUNDING POLYIMIDE POLYMER

Many factors influence the load transfer efficiency, such as the non-bonded atomistic interaction, surface modification of SWCNTs and covalent bonding between the SWCNTs and matrix. In this chapter, the SWCNTs/polyimide nanocomposites with various interfacial adhesions were constructed. After the simulation models were constructed, an axial loading was applied to the nanocomposite models and the stress distribution was obtained using atomic level stress formulation and the derivative of the potential function. In addition, the influence of the atomistic interactions between the SWCNTs and the surrounding polyimide on the load transfer efficiency as well as the corresponding tensile moduli of nanocomposites were also discussed.

4.1 Establishment of the SWCNTs/Polyimide Nanocomposites with Different Interfacial Adhesions

4.1.1 Molecular structures of SWCNTs/polyimide nanocomposites

To investigate the stress distribution of SWCNTs, the molecular structure of nanocomposites, which consist of SWCNTs and polyimide polymer, was constructed as shown in Fig. 4-1. The (10, 0) zig-zag SWCNTs with radius of 3.9 Å and length of 42.6 Å were considered as a reinforcement embedded in the polyimide nanocomposites, while the polyimide containing 32 molecular chains was regarded as the polymer matrix. Each polyimide molecular chain was generated by 10 monomer units. To understand the influences of atomistic interaction on the load transfer efficiency as well as the modulus of the nanocomposites, three different interfacial adhesions between the SWCNTs and polyimide polymer were considered; non-bonded vdW interaction, SWCNTs with surface modification and covalent bonding. The vdW interaction is always taking place between the SWCNTs and polyimide polymer when SWCNTs with surface modification and covalent bond were considered in the simulation. For the SWCNTs with surface modification,   8 polyethylene

polymer chains (C_5H_{11}) adhered axial-symmetrically on the SWCNTs surface as shown in Fig. 4-2. Such an arrangement of polyethylene chains is to allow for the easy exploration into the influence of surface modification on the stress distribution of the SWCNTs. With regard to the covalently bonded interaction, the polyethylene chains originally adhered to the SWCNTs surface were further covalently bonded to the polyimide molecular chains. The connection was established by the covalent bonds between the carbon atoms at the ends of polyethylene chains and the carbon atoms in the polyimide chains. As a result, the interatomistic relation between CNTs and the surrounding polyimide matrix involves not only vdW forces but also the covalence bond interactions.

4.1.2 Potential function

In the molecular model of SWCNT/polyimide nanocomposites, atomistic interactions between SWCNTs and polyimide polymers were constructed, based on the previous section. In regions of interfacial adhesion, the L-J potential was adopted to model the atomistic interaction between SWCNTs and the polymer for which the corresponding parameters were referred to as the Dreiding force field [36]. In addition, four different intensities of vdW interaction between the SWCNTs and surrounding polyimide polymer, 0.01, 0.1, 1 and 5x, were considered to investigate the influence of the intensity of vdW interaction on load transfer efficiency. For the SWCNT surface modification, to consider the consistency of force field between the SWCNTs and polyethylene, AMBER force fields [34] were adopted to simulate the potentials of Polyethylene polymers. The surface of SWCNTs is chemically modified by polyethylene polymers; therefore, carbon atoms on the SWCNTs, which were bonded with polyethylene polymer, were changed from sp^2 to sp^3 hybridized carbon atoms. With regard to the interface of covalently bonded, the potential of the covalent bonds at the interface between the carbon atoms at the ends of the polyethylene chains and the carbon atoms in the polyimide chains were also constructed by AMBER force field [34].

4.1.3 Molecular dynamics simulation processes

The equilibrated molecular structure of SWCNTs/polyimide nanocomposites with minimized energy was generated by sequentially performing MD simulations with the NVT and NPT ensembles with a time increment of 1 fs. In the NVT ensemble, the carbon atoms on SWCNTs were fixed at their original position throughout the whole simulation [30]. The NPT process was set to 0 atm so that the simulation box with a stress-free boundary condition could be achieved. Three sub-steps were introduced into the NPT process for the temperature reduction from 1000 to 0 K. In the first and second steps, the temperature was set at 600 K and 300K respectively, and the simulation time for each step was 200 ps with a time increment of 1 fs. For the third step, a modified NPT ensemble was employed to obtain the molecular structures of nanocomposites with stress-free condition. During the modified NPT ensemble, the frozen SWCNT atoms in the nanocomposites were released and the corresponding temperature was set at 0 K. During the simulation, the total potential energy variation was examined, and after the quantity fluctuated around a certain mean value for a while, the system was considered to be in equilibrium. Figs. 4-3 and 4-4 demonstrate the potential energy history of the nanocomposites as well as the temperature variations during the third step in the NPT ensemble, respectively. The potential energy reaches a stable level after 100 ps, and the temperature approaches 0 K. Based on these observations, the current molecular structure is considered to be at equilibrium. Fig. 4-1 illustrates the molecular structure of SWCNT/polyimide nanocomposites. The uniaxial loading (0.01 GPa) was applied at the boundary of the simulation box in the Z direction as shown in Fig. 4-5. The corresponding equilibrated molecular structure subjected to uniaxial loading was obtained after MD simulation of the modified NPT ensemble with a time increment of 1 fs over 200 ps. After the tensile process, the equilibrated molecular structure under uniaxial loading was obtained and the stress history in various directions for the modified NPT ensemble is shown in Fig. 4-6.

4.1.4 Density distribution

The density distribution of polyimide polymer near the SWCNTs was initially examined using Eq. (3.1). Fig. 4-7 shows the density distribution of polyimide polymer in the radial direction for different degrees of vdW interactions. The polymer density is relatively high near the SWCNTs, and then declines to a normal value of 1.31 g/cc [49] at locations further from the SWCNTs. Furthermore, the phenomenon of high polymer density around the SWCNTs is more significant when the vdW intensity strengthens. The density distribution in the polyimide polymer is influenced by the presence of SWCNTs and the high density polyimide may play an essential role in the load transfer efficiency of the nanocomposites.

4.2. Stress Calculations

4.2.1 Definition of various atomic level stress formulations

The most widely used stress measured at the atomic scale is the virial stress and is expressed as:

$$\sigma_{ij}^{virial} = -\frac{1}{V^{Total}} \left\{ \sum_{\alpha=1}^{N} m^{\alpha} v_i^{\alpha} v_j^{\alpha} + \frac{1}{2} \sum_{\alpha=1}^{N} \sum_{\beta \neq \alpha}^{N} r_i^{\alpha\beta} F_j^{\alpha\beta} \right\} \tag{4.1}$$

In Eq. (4.1), m^{α} and $\mathbf{v}^{\alpha}$ v_i^{α} represent the mass and velocity of atom α respectively, and $\mathbf{r}^{\alpha\beta} = \mathbf{r}^{\alpha} - \mathbf{r}^{\beta}$ $r_i^{\alpha\beta} = r_i^{\alpha} - r_i^{\beta}$ where $\mathbf{r}^{\alpha}$ r_i^{α} and $\mathbf{r}^{\beta}$ r_i^{β} denote the positions of atom α and β respectively. $\mathbf{F}^{\alpha\beta}$ $F_j^{\alpha\beta}$ is the internal force between atom α and atom β. V^{Total} is the volume of the simulation box and N is the number of atoms within the simulation box. According to the previous discussion regarding volume, the virial stress is a homogeneous stress resulting from the entire volume of the simulation box. Basically, the virial stress provides the averaged stress state in the simulation box rather than the "local" stress state [57].

By focusing on the atomistic interaction of the atom α with other atoms, the local stress of atom α was derived as [58]

$$\sigma_{ij}^{BDT} = -\frac{1}{V^\alpha} \left\{ m^\alpha v_i^\alpha v_j^\alpha + \frac{1}{2} \sum_{\beta \neq \alpha}^{N} r_i^{\alpha\beta} F_j^{\alpha\beta} \right\} \tag{4.2}$$

The above expression is the so-called BDT stress proposed by Basinski et al. [58]. In the BDT stress expression, V^α indicates the atomistic volume of atom α. For the CNTs, the atomistic volume is considered as $V^\alpha = \dfrac{V^{CNT}}{N^{CNT}}$ where $V^{CNT} = \pi D_0 t L_0$ is the volume of the SWCNTs, and N^{CNT} is the number of atoms within the SWCNTs. L_0 is the length of SWCNTs and t=3.4 Å is the wall thickness of the SWCNTs and D_0 is the diameter of the SWCNTs.

Lutsko stress was proposed by Lutsko [28] and extended by Cormier et al. [29] and is based on the local stress tensor of statistical mechanics. Lutsko stress assumes that the stress state is homogeneous over the entire averaged volume and can be expressed as

$$\sigma_{ij}^{Lutsko} = -\frac{1}{V^{Lutsko}} \left\{ \sum_{\alpha=1}^{N} m^\alpha v_i^\alpha v_j^\alpha + \frac{1}{2} \sum_{\alpha=1}^{N} \sum_{\beta \neq \alpha}^{N} r_i^{\alpha\beta} F_j^{\alpha\beta} l^{\alpha\beta} \right\} \tag{4.3}$$

where V^{Lutsko} is the average volume for the Lutsko stress formulation and $l^{\alpha\beta}$ denotes the fraction of the length of the α–β bond lying inside the average volume. In general, Lutsko stress formulation provides the averaged value of the stress within the selected volume. Because of the geometry of SWCNTs, the cylindrical shape was considered in this paper as an average volume and is shown in Fig. 4-8 and V^{Lutsko} is written as

$$V^{\text{Lutsko}} = \pi D_0 t L_{\text{Lutsko}} \qquad\qquad\qquad (4.4)$$

where L_{Lutsko} is the length of average volume and is equal to 10Å for this research.

4.2.2 Applicability of atomic stress formulation

In order to validate the applicability of the various formulae for atomic level stress on SWCNTs, the SWCNTs with stress-free and uniaxial loading states were constructed by MD simulation, and the stress distribution of the SWCNTs with stress-free and uniaxial loading states were then calculated by atomic level stress formulations. Finally, the stress results from the various stress formulations were compared for an applied loading on SWCNTs.

The molecular structure of (10, 0) CNTs with radius 3.9 Å and length 42.6 Å, was employed for the demonstration. Both bonded and non-bonded interactions were accounted for in the carbon atoms. Through an energy minimization process, the SWCNTs in the stress-free state were obtained. The atoms at one end of the SWCNTs were then fixed while a small axial displacement (0.0426Å) was applied to the atoms located at the other end of SWCNTs as shown in Fig. 4-9. Again, the energy minimization process at zero temperature was performed and the deformed configuration of SWCNTs was obtained. The stress generated within the SWCNTs and the corresponding value can be evaluated from the BDT stress [57] and Lutsko stress [28, 29]. In addition to atomic level stress formulations, the stress distribution of the SWCNTs can also be calculated directly from the atomistic interactions between the carbon atoms associated with the bonded and non-bonded potentials. An imaginary plane through the cross section of SWCNTs was assumed and the possible atomistic interactions passing through this imaginary plane were then calculated in terms of the potential functions. The simulation was performed at 0K, the kinetic energy was disregarded, and only the potential energy was considered in the stress calculation. Fig. 4-10

illustrates the imaginary plane of the SWCNTs. By taking the derivative of the potential function, the forces F_{int} going through the imaginary plane can be obtained and the stress can be calculated accordingly as

$$\sigma_{int} = \frac{F_{int}}{A} \qquad (4.5)$$

where A is the cylindrical cross section of SWCNTs. The stress distributions of SWCNTs in the stress-free state as well as in the deformed configuration were calculated based on the atomic level stress formulations and potential functions, and the results are compared in Figs. 4-11 and 4-12, respectively.

From Fig. 4-11, the axial stress of SWCNTs calculated based on Lutsko stress formulation and the derivative of the potential function are equal to zero all the way through the SWCNTs; however, for the BDT stress, some oscillations exist near the ends of the SWCNTs. The nonphysical phenomenon also appeared in Ref. [57]. For the SWCNTs under axial deformation, Fig. 4-12 shows that the stress calculated from the derivative of the potential function is uniform along the SWCNTs and the corresponding value is equal to the applied loading. However, for the Lutsko stress, although the stress value remains constant in the middle portion, it begins to drop near the ends of the SWCNTs. This decrease is because at the ends of SWCNTs, only some of the atomistic interactions were included in the average volume V^{Lutsko} for the stress calculation. In addition, for the BDT stress, the stress fluctuation was still observed near the ends of SWCNTs. In light of the forgone discussion, the Lutsko stress formula and the stress field based on the derivative of the potential functions are capable of exhibiting the stress distribution of the deformed SWCNTs. Therefore, both approaches were employed to calculate the stress distribution of the SWCNTs embedded in the nanocomposites when the nanocomposites are subjected to axial loading.

4.3 Stress Distribution over the SWCNTs in the Nanocomposites

4.3.1 Mechanism of load transfer

When the equilibrated molecular structure of SWCNT/polyimide nanocomposites was obtained as shown in Fig. 4-1, the axial stress distribution in the pristine SWCNTs was evaluated by Lutsko stress formulation and potential function. Fig. 4-13 shows the axial stress distribution of the pristine SWNCTs for a 1x vdW interaction when the nanocomposites were in the stress-free state. Compressive residual stress was observed in the SWCNTs. The reason for residual stress is that SWCNTs interact with surrounding polymers by interfacial interaction when pristine SWCNTs embed in the polymers. Due to the residual stress effect, observing the variation in stress distribution is difficult for the SWCNTs when nanocomposites are subjected to the applied loading. Hence, the stress distribution of SWCNTs with the deformed configurations of nanocomposites, subtracted from its residual stress phenomenon, was obtained via Lutsko stress formulation and the potential function shown in Fig. 4-14. The axial stress is distributed almost uniformly along the SWCNTs. This phenomenon suggested that the load is transferred to the SWCNTs mostly through both ends rather than by means of the SWCNTs wall surface.

To further verify the behavior of load transfer, the external forces on SWCNTs atoms were calculated from the non-bonded interaction between the SWCNTs and surrounding polymer. The external force distributions of SWCNTs were obtained when nanocomposites with 1x vdW interaction were in the stress-free state as well as the loading state, and the results are presented in Figs. 4-15 and 4-16, respectively. As seen in Fig. 4-15, SWCNTs were subjected to relatively high compressive loading at both ends. The values of external force are close to zero in the SWCNTs except at both ends. Fig. 4-16 shows that SWCNTs were subjected to relatively high tensile loading at both ends and the values of axial external force were close to zero near at the center of the SWCNTs. Based on these phenomena, we can confirm that the load was transferred to the SWCNTs mostly through both ends of the

SWCNTs rather than through the SWCNT wall surface.

4.3.2 Influences of interfacial adhesions

To explore the influences of interfacial adhesions on the load transfer efficiency as well as the mechanical properties of nanocomposites, the stress distribution of the SWCNTs with a deformed configuration of nanocomposites was calculated using the Lutsko stress formulation and the potential function. Fig. 4-17 shows the load transfer from the surrounding matrix to the SWCNTs for the different degrees of vdW interaction. As the vdW interaction strengthens, the corresponding stress field in the SWCNTs is accordingly higher, implying that the load transfer from the polyimide to the SWCNTs is more efficient. In addition, it is observed that the axial stress is distributed almost uniformly along the SWCNTs. This phenomenon suggested that the load is transferred to the SWCNTs mostly through both ends of the SWCNTs rather than through the SWCNTs wall surface. Moreover, the moduli of the SWCNT nanocomposites associated with different intensities of vdW are summarized in Table 4-1. The moduli of the nanocomposites are also improved with an increase in vdW interactions. Because the stress fields shown in Fig. 4-17 were calculated based on Lutsko stress formulation, a perceptible stress drop near the ends of the SWCNTs is observed. After we evaluated the stress distributions using the potential function approach, no significant stress drop near the ends were observed, as seen in Fig. 4-18. The almost uniform stress distribution again validates the fact that the load was transferred into the SWCNTs mostly through the ends. In addition to the vdW interactions, the surface modification on the SWCNTs as well as the covalent bonds were regarded as the interfacial properties between the SWCNTs and polyimide. Fig. 4-19 illustrates the stress distribution of the SWCNTs associated with three different interfacial adhesions. The corresponding moduli of the nanocomposites are also presented in Table 4-2. They illustrate that the SWCNTs with surface modification exhibit both a higher load transfer efficiency and higher nanocomposite

38

moduli of compared to the other two cases. The improvement caused by the surface modification could be due to the entangle effect between the polyethylene surfactant and the polyimide matrix. When the nanocomposites are subjected to loading, a relative deformation takes place at the interface because of the mismatch between the constituent materials. If the interfacial bonding is weak, the relative displacement is large and the load transfer efficiency is relatively lower. However, if the interfacial bonding strengthens, the relative displacement is less and the load transfer efficiency is increased. The purpose of the polyethylene surfactant is to increase "friction" between the SWCNTs and polyimide matrix and meanwhile reduce the relative displacement so that the load can be effectively transferred onto the SWCNTs. The effect of the polyethylene surfactant is clearly demonstrated in Fig. 4-20, in which the stress curves were calculated based on the potential approach. The stresses show a dramatic rise around the positions where the surfactants were attached to the SWCNTs (indicated by the dash line). In addition, both the covalent bonding and the surface modification were shown to provide the same enhancement in load transfer efficiency in the nanocomposites. In other words, the function of covalent bond was not completely demonstrated in the current simulation.   There are several factors causing the results, i.e., the size of the simulation box, the connection of the covalent bond, and the selection of surfactant. Details regarding the influence of covalent bonding on the mechanical responses of nanocomposites will be examined in the near future.

CHAPTER 5 CONCLUSION

The mechanical properties of the SWCNT/polyimide nanocomposites were characterized using multi-scale simulation. An equivalent cylindrical solid was proposed to model the atomistic structure of SWCNTs, and the corresponding properties were determined from the molecular mechanics in conjunction with the energy equivalence concept. The level of atomistic interaction between the SWCNTs and the surrounding polyimide polymer was modeled by an effective interphase, the properties of which were obtained from the non-bonded energy as well as the non-bonded gap as determined from the MD simulation. With the properties of the equivalent solid cylinder, effective interphase, and polyimide polymer, the mechanical properties of SWCNTs nanocomposites can be predicted using the three-phase continuum micromechanical model. For comparison purposes, the two-phase micromechanical model (Mori–Tanaka model) was also adopted for the predictions. A comparison between the micromechanical results and the MD results indicates that the longitudinal moduli of the SWCNT nanocomposites can be precisely predicted using the two-phase micromechanical model together with the equivalent cylinder properties of the SWCNTs. However, in the transverse direction, the three-phase model can provide improved results over the two-phase micromechanical model because the atomistic interactions between the SWCNTs and polyimide polymer become essential for such conditions.

In addition, the relationship of the load transfer efficiency of SWCNT/polyimide nanocomposites to the three different interfacial adhesions, vdW interactions, SWCNTs surface modifications and covalent bonds, was investigated in this study. Both the Lutsko stress formulation and the derivative of the potential function approach were employed to calculate the stress distribution of the SWCNTs embedded in polyimide nanocomposites. Results indicate that when the intensities of vdW interactions increase, the load transfer efficiency and the moduli of the nanocomposites increase accordingly. In addition, the surface

modification of SWCNTs showed to be an effective way to improve the load transfer efficiency as well as the mechanical properties of nanocomposites. Due to the limited size of the molecular structures, the effect of covalent bonds is almost the same as that of the surface modification. Further study is required to understand the influence of the covalent bonds on the mechanical properties of nanocomposites.

References

1. Iijima S. Helical microtubules of graphitic carbon. Nature. 1991; 354(6348): 56-58.

2. Gibsion RF. Principles of composite material mechanics. 1994, New York: McGraw-Hall Inc.

3. Lau KT, Gu C, Hui D. A critical review on nanotube and nanotube/nanoclay related polymer composite materials. Compos Part B-Eng. 2006; 37(6): 425-436.

4. Thostenson ET, Ren Z, Chou TW. Advances in the science and technology of carbon nanotubes and their composites: a review. Compos Sci Technol. 2001; 61(13): 1899-1912.

5. Han Y, Elliott J. Molecular dynamics simulations of the elastic properties of polymer/carbon nanotube composites. Comp Mater Sci. 2007; 39(2): 315-323.

6. Griebel M, Hamaekers J. Molecular dynamics simulations of the elastic moduli of polymer-carbon nanotube composites. Comput Methods Appl Mech Eng. 2004; 193(17-20): 1773-1788.

7. Zhu R, Pan E, Roy AK. Molecular dynamics study of the stress-strain behavior of carbon-nanotube reinforced Epon 862 composites. Mater Sci Eng A. 2007; 447(1-2): 51-57.

8. Liu YJ, Chen XL. Evaluations of the effective material properties of carbon nanotube-based composites using a nanoscale representative volume element. Mech Mater. 2003; 35(14): 69-81.

9. Luo D, Wang WX, Takao Y. Effects of the distribution and geometry of carbon nanotubes on the macroscopic stiffness and microscopic stresses of nanocomposites. Compos Sci Technol. 2007; 67(14): 2947-2958.

10. Selmi A, Friebel C, Doghri I, Hassis H. Prediction of the elastic properties of single walled carbon nanotube reinforced polymers: A comparative study of several micromechanical models. Compos Sci Technol. 2007; 67(10): 2071-2084.

11. Hammerand DC, Seidel GD, Lagoudas DC. Computational micromechanics of clustering and interphase effects in carbon nanotube composites. Mech Adv Mater Struct. 2004; 14(4): 277-294.

12. Gates TS, Odegard GM, Frankland SJV, Clancy TC. Computational materials: multi-scale modeling and simulation of nanostructured materials. Compos Sci Technol. 2005; 65(15-16): 2416-2434.

13. Shim BS, Zhu J, Jan E, Critchley K, Ho S, Podsiadlo P, Sun K, Kotov NA. Multiparameter structural optimization of single-walled carbon nanotube composites: toward record strength, stiffness, and toughness. ACS Nano. 2009; 3(7): 1711-1722.

14. Mokashi VV, Qian D, Liu Y. A study on the tensile response and fracture in carbon nanotube-based composites using molecular mechanics. Compos Sci Technol. 2007; 67(3-4): 530-540.

15. Yavin B, Gallis HE, Scherf J, Eitan A, Wagner HD. Continuous monitoring of the fragmentation phenomenon in single fiber composite materials. Polym Composite. 1991; 12(6): 436-446.

16. Andersons J, Joffe R, Hojo M, Ochiai S. Fibre fragment distribution in a single-fibre composite tension test. Compos Part B-Eng. 2001; 32(4):323-332.

17. Valadez-Gonzalez A, Cervantes-Uc JM, Olayo R, Herrera-Franco PJ. Effect of fiber surface treatment on the fiber-matrix bond strength of natural fiber reinforced composites. Compos Part B-Eng. 1999; 30(3): 309-320.

18. Moon CK. The effect of interfacial microstructure on the interfacial strength of glass fiber/polypropylene resin composites. J Appl Polym Sci. 1994; 54(1): 73-82.

19. Piggott MR, Dai SR. Fiber pull out experiments with thermoplastics. Polym Eng Sci. 1991; 31(17):1246-1249.

20. Al-Haik M, Hussaini MY, Garmestani H. Adhesion energy in carbon nanotube-polyethylene composite: Effect of chirality. J Appl Phys. 2005; 97(7): 074306.

21. Namilae S, Chandra N. Multiscale model to study the effect of interfaces in carbon nanotube-based composites. J Eng Mater-T ASME. 2005; 127(2): 222-232.

22. Gou J, Minaie B, Wang B, Liang Z, Zhang C. Computational and experimental study of interfacial bonding of single-walled nanotube reinforced composites. Comp Mater Sci. 2004; 31(3-4): 225-236.

23. Lordi V, Yao N. Molecular mechanics of binding in carbon-nanotube polymer composites. J Mater Res. 2000; 15(12): 2770-2779.

24. Frankland SJV, Caglar A, Brenner DW, Griebel M. Molecular simulation of the influence of chemical cross-links on the shear strength of carbon nanotube-polymer interfaces. J Phys Chem B. 2002; 106(12): 3046-3048.

25. Chowdhury SC, Okabe T. Computer simulation of carbon nanotube pull-out from polymer by the molecular dynamics method. Compos Part A-Appl S. 2007; 38(3): 747-754.

26. Zheng Q, Xia D, Xue Q, Yan K, Gao X, Li Q. Computational analysis of effect of modification on the interfacial characteristics of a carbon nanotube-polyethylene composite system. Appl Surf Sci. 2009; 255(6): 3534-3543.

27. Li C, Chou TW. Multiscale modeling of carbon nanotube reinforced polymer composites. J Nanosci Nanotechno. 2003; 3(5): 423-430.

28. Lutsko JF. Stress and elastic constants in anisotropic solids: Molecular dynamics techniques. J Appl Phys. 1988; 64(3): 1152-1154.

29. Cormier J, Rickaman JM, Delph TJ. Stress calculation in atomistic simulations perfect and imperfect solids. J Appl Phys. 2001; 89(1): 99-104.

30. Suzuki K, Nomura S. On elastic properties of single-walled carbon nanotubes as composite reinforcing fillers. J Compos Mater. 2007; 41(9): 1123-1135.

31. Lau KT, Chipara M, Ling HY, Hui D. On the effective elastic moduli of carbon nanotubes for nanocomposite structures. Composites B. 2004; 35(2): 95-101.

32. Rappe AK, Casewit CJ. Molecular mechanics across chemistry. Sausalito, California: University Science Books; 1997.

33. Li C, Chou TW. A structural mechanics approach for the analysis of carbon nanotubes. Int J Solids Struct. 2003; 40(10): 2487-2499.

34. Cornell WD, Cieplak P, Bayly CI, Gould IR, Merz Jr KM, Ferguson DM, Spellmeyer DC, Fox T, Caldwell JW, Kollman PA. A second generation force field for the simulation of proteins, nucleic acids, and organic molecules. J Am Chem Soc. 1995; 117(19): 5179-5197.

35. Smith W, Forester TR. DLPOLY-2.13 manual. 2001.

36. Mayo SL, Olafson BD, Goddard III WA. DREIDING: a generic force field for molecular simulations. J Phys Chem. 1990; 94(26): 8897-8909.

37. Xiao JR, Gama BA, Gillespie Jr. JW. An analytical molecular structural mechanics model for the mechanical properties of carbon nanotubes. Int J Solids Struct. 2005; 42(11-12): 3075-3092.

38. Agrawal PM, Sudalayandi BS, Raff LM, Komanduri R. A comparison of different methods of Young's modulus determination for single-wall carbon nanotubes (SWCNT) using molecular dynamics (MD) simulations. Comp Mater Sci. 2006; 38(2): 271-281.

39. Chen WH, Cheng HC, Hsu YC. Mechanical properties of carbon nanotubes using molecular dynamics simulations with the inlayer van der waals interactions. CMCS. 2007; 20(2): 123-145.

40. Krishnan A, Dujarin E, Ebbesen TW, Yianilos PN, Treacy MMJ. Young's modulus of single-walled nanotubes. Phys Rev B. 1998;58(20):14013-14019.

41. Battezzatti L, Pisani C, Ricca F. Equilibrium conformation and surface motion of hydrocarbon moleculars physisorbed on graphite. J Chem Soc. 1975; 71: 1629-1639.

42. Tserpes KI, Papanikos P. Finite element modeling of single-walled carbon nanotubes. Composites B. 2005; 36(5): 468–477.

43. Wang Y, Wang XX, Ni X. Atomistic simulation of the torsion deformation of carbon nanotubes. Modell Simul Mater Sci Eng. 2004; 12(6): 1099-1107.

44 Gere JM. Mechanics of materials. 5th ed. Cheltenham, UK: Nelson Thornes; 2001.

45. Melchionna S, Ciccotti G, Holian BL. Hoover NPT dynamics for systems varying in shape and size. Mol Phys. 1993; 78(3): 533-544.

46. Mori T, Tanaka K. Average stress in matrix and average elastic energy of materials with misfitting inclusions. Acta Metall. 1973; 21(5): 571-574.

47. Allen MP, Tildesley DJ. Computer simulation of liquids. Oxford: Clarendon Press; 1987.

48. Adnan A, Sun CT, Mahfuz H. A molecular dynamics simulation study to investigate the effect of filler size on elastic properties of polymer nanocomposites. Compos Sci Technol. 2007; 67(3–4):3 48–56.

49. Ashby MF, Jones DR. Engineering materials 1: an introduction to their properties and applications. Oxford: Butterworth; 1996.

50. Gedde, UW. Polymer physics. 1995, Chapman and Hall, London.

51. Shames IH, Cozzarelli FA. Elastic and Inelastic Stress Analysis. 1992. Prentice-Hall, New Jersey.

52. Dunn ML, Ledbetter H. Elastic moduli of composites reinforced by multiphase particles. J Appl Mech 1995;62(4):1023-1028.

53. Hori M, Nemat-Nasser S. Double-inclusion model and overall moduli of multiphase composites. Mech Mater 1993;14(3):189-206.

54. Eshelby JD. The determination of the elastic field of an ellipsoidal inclusion, and related problems. Proc R Soc Lond Ser A. 1957;241(1226):376-396.

55. Qiu YP, Weng GJ. On the application of Mori-Tanaka's theory involving transversely isotropic spheroidal inclusions. Int J Eng Sci. 1990; 28(11): 1121-1137.

56. Cadek M, Coleman JN, Ryan KP, Nicolosi V, Bister G, Fonseca A, Nagy JB, Szostak K, Béguin F, Blau WJ. Reinforcement of polymers with carbon nanotubes: the role of nanotube surface area. Nano Lett. 2002;4(2):353–356.

57. Sun ZH, Wang XX, Soh AK, Wu HA. On stress calculations in atomistic simulations. Modelling Simul Mater Sci Eng. 2006; 14(3): 423-431.

58. Basinski ZS, Duesbery MS, Taylor R. Influence of shear stress on screw dislocations in a model sodium lattice. Can J Phys. 1971;49(16):2160-2180.

Table 2-1. The effect of van der Waals force on axial Young's modulus of the SWCNTs with three different radii.

Radius(Å)	Young's modulus with van der Waals force (GPa)	Young's modulus without van der Waals force (GPa)
3.9	790.56	794.11
5.5	791.71	793.84
7.1	790.45	792.09

Table 2-2. Mechanical properties of equivalent solid cylinder with three different CNT radii.

Radius(Å)	E_1 (GPa)	G_{12} (GPa)	ν_{12}	E_2 (GPa)	ν_{23}
3.9	1382.5	1120	0.272	645	0.2
5.5	981.5	779.2	0.27	504	0.2
7.1	759.9	596.3	0.27	425	0.2

Table 2-3. The transverse properties of equivalent solid cylinder with three different CNTs radii.

Radius(Å)	E_2 (GPa)	ν_{23}
3.9	645	0.2
	483	0.4
5.5	504	0.2
	377	0.4
7.1	425	0.2
	319	0.4

Table 2-4. Two different mechanical property groups of equivalent solid cylinder.

	E_1 (GPa)	G_{12} (GPa)	ν_{12}	E_2 (GPa)	ν_{23}
Material 1	1382.5	1120	0.272	645	0.2
Material 2	1382.5	1120	0.272	483	0.4

Table 2-5. Mechanical properties of nanocomposites based on different mechanical property groups of equivalent solid cylinder.

	E_1 (GPa)	E_2 (GPa)	G_{12} (GPa)	G_{23} (GPa)	ν_{12}
Composites 1	113.98	4.54	1.79	1.9	0.3
Composites 2	113.98	4.51	1.8	1.9	0.3

Table 3-1. Non-bond gap and normalized non-bonded energy in SWCNTs/polyimide nanocomposites with various CNTs radii.

Radius(Å)	Non-bond gap (Å)	Normalized non-bonded energy (j/m^2)
3.9	3.333	0.3560
5.5	3.236	0.3269
7.1	3.158	0.3142

Table 3-2. The elements in the stiffness matrix for the SWCNTs/polyimide nanocomposites calculated from MD simulation.

Radius(Å)	C_{11}(GPa)	C_{22}(GPa)	C_{33}(GPa)	C_{12}(GPa)	C_{13}(GPa)	C_{23}(GPa)
3.9	95.47	10.39	11.14	6.645	6.45	6.95
5.5	72.79	10.47	10.83	6.745	6.965	7.235
7.1	59.14	10.15	10.39	6.75	6.52	7.10

Table 3-3. The elements in the stiffness matrix for the neat polyimide polymer calculated from MD simulation.

	C_{11}(GPa)	C_{22}(GPa)	C_{33}(GPa)	C_{12}(GPa)	C_{13}(GPa)	C_{23}(GPa)
Polyimide	8.89	8.92	9.54	6.245	6.375	6.175
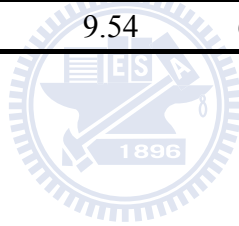
Table 3-4. Material properties of neat polyimide polymer.

	E(GPa)	ν
Polyimide	4.01	0.407

Table 3-5. Comparing of longitudinal moduli of SWCNTs/polyimide nanocomposites obtained from MD simulation, Mori-Tanaka model and three-phase model.

Radius(Å)	Volume fraction (%)	MD simulation (GPa)	Mori-Tanaka Model (GPa)	Three-phase model (GPa)
3.9	6.28	90.6	90.6	92.9
5.5	6.43	56.6	66.9	54.7
7.1	6.67	54.2	54.7	55.8

Table 3-6. Comparing of transverse moduli of SWCNTs/polyimide nanocomposites obtained from MD simulation, Mori-Tanaka model and three-phase model.

Radius(Å)	Volume fraction (%)	MD simulation (GPa)	Mori-Tanaka Model (GPa)	Three-phase model (GPa)
3.9	6.28	6.22	5.28	6.32
5.5	6.43	5.86	5.27	5.90
7.1	6.67	5.29	5.28	5.74

Table 4-1. Comparison of longitudinal moduli of CNTs/polyimide nanocomposites with different degrees of vdW interactions.

Degrees of vdW interaction	Longitudinal modulus (GPa)
0.01 vdW	4.196
0.1 vdW	4.212
1 vdW	4.295
5 vdW	4.91

Table 4-2. Comparison of longitudinal moduli of CNTs/polyimide nanocomposites with different interfacial adhesions.

Interfacial adhesions	Longitudinal modulus (GPa)
vdW interaction	4.3
Surface modification	4.52
Covalent bond	4.41
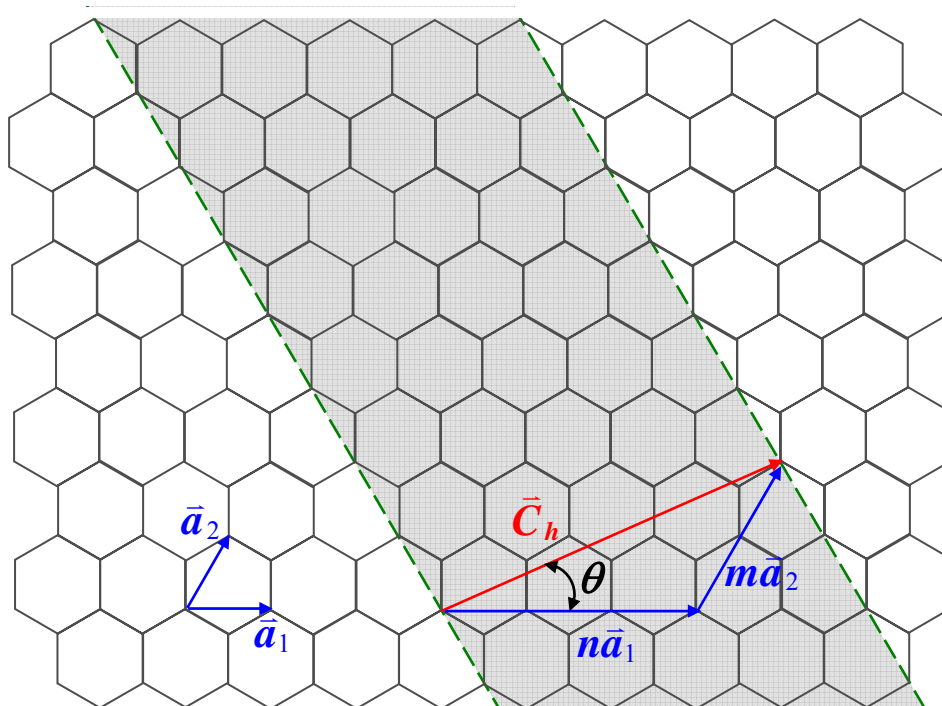
Figure 1-1.   2D graphene sheet with nanotube parameter.
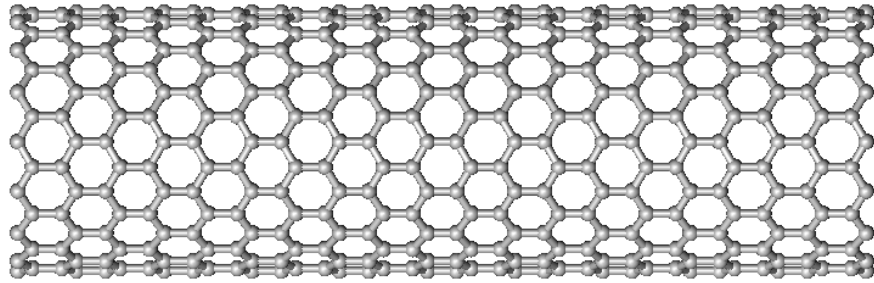
(a)

(b)

(c)
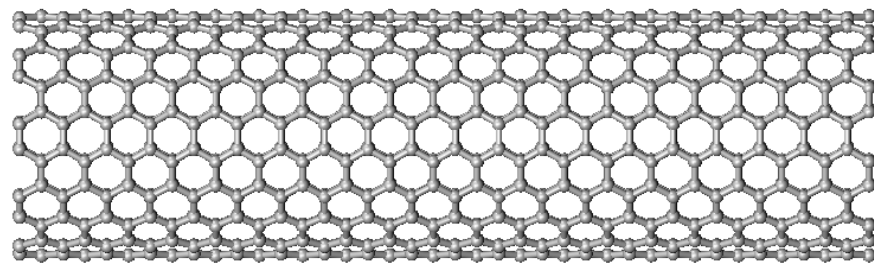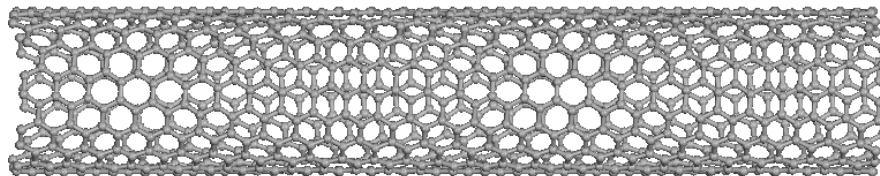
Figure 1-2. Illusion of the atomic structure of an (a) an armchair, (b) a zigzag and (c) a chiral nanotube.
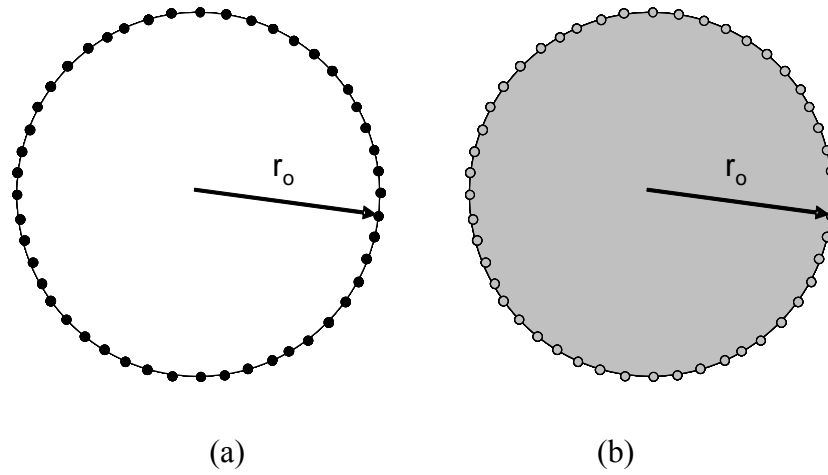
Figure 2-1. Schematic of SWCNTs cross-section (a) cylindrical shell model (b) cylindrical solid model
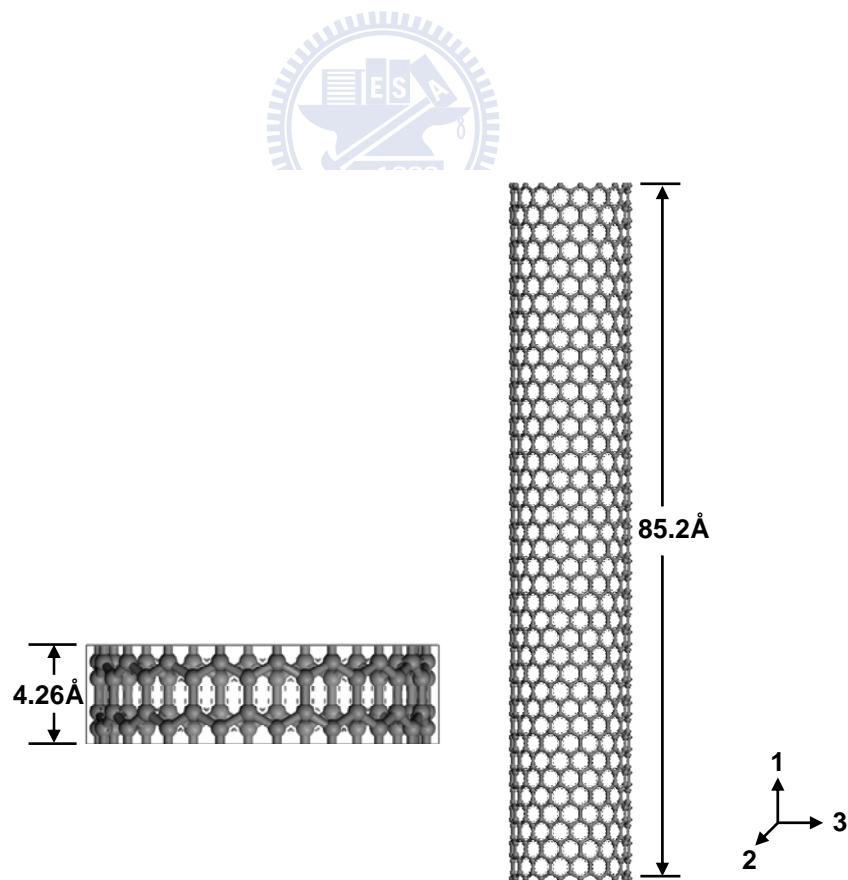
Figure 2-2. Schematic of zigzag type (18,0) SWCNTs unit cell.
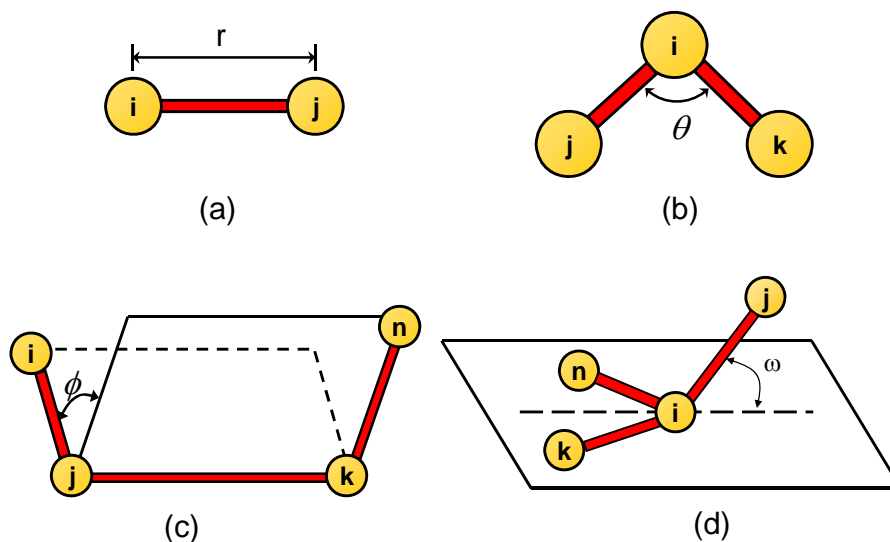
Figure 2-3. A schematic representation of the inter-atomic potential (a) bond stretch, (b) angle potential, (c) dihedral potential, and (d) inversion potential.
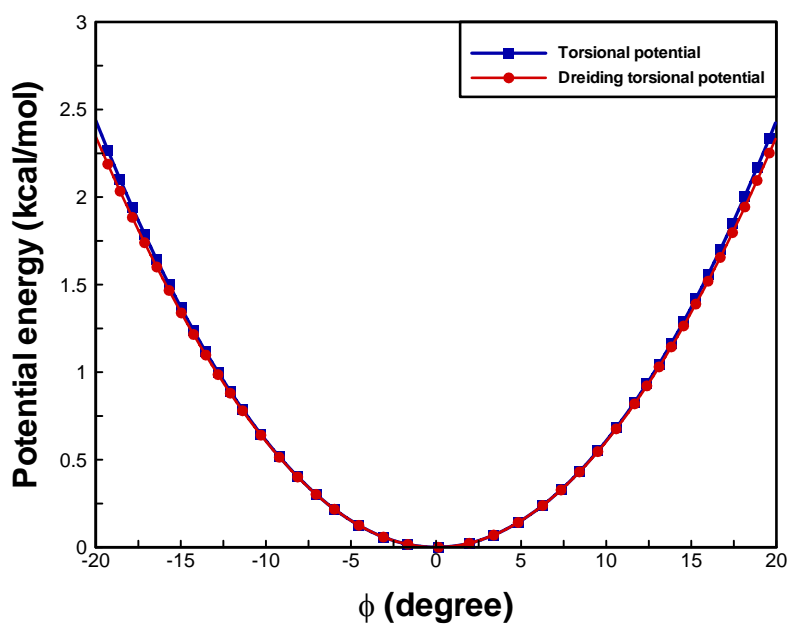
Figure 2-4. Comparing the torsional potential (Eq. 2.4) with Dreiding torsional potential (Eq. 2.5).
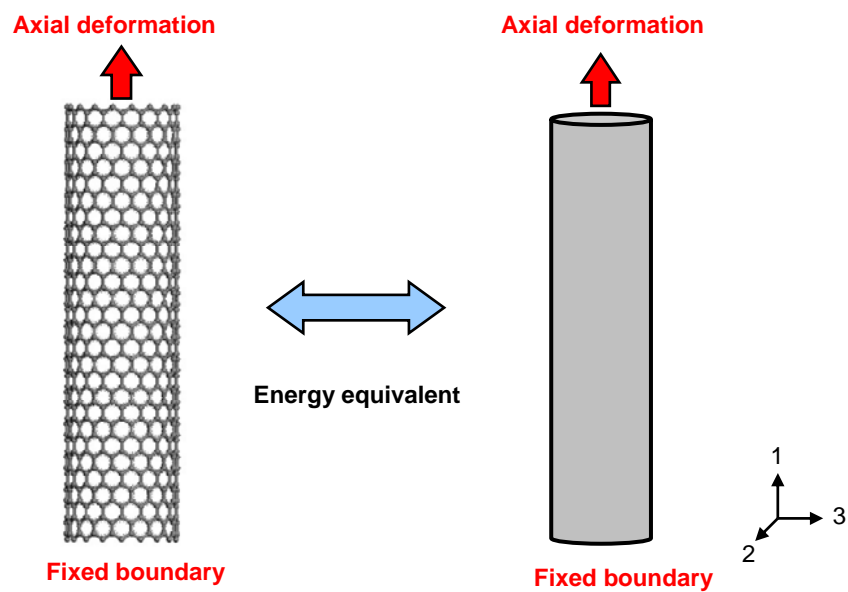
Figure 2-5. Axial deformation was applied to the SWCNTs atomistic structures and the equivalent solid cylinder.
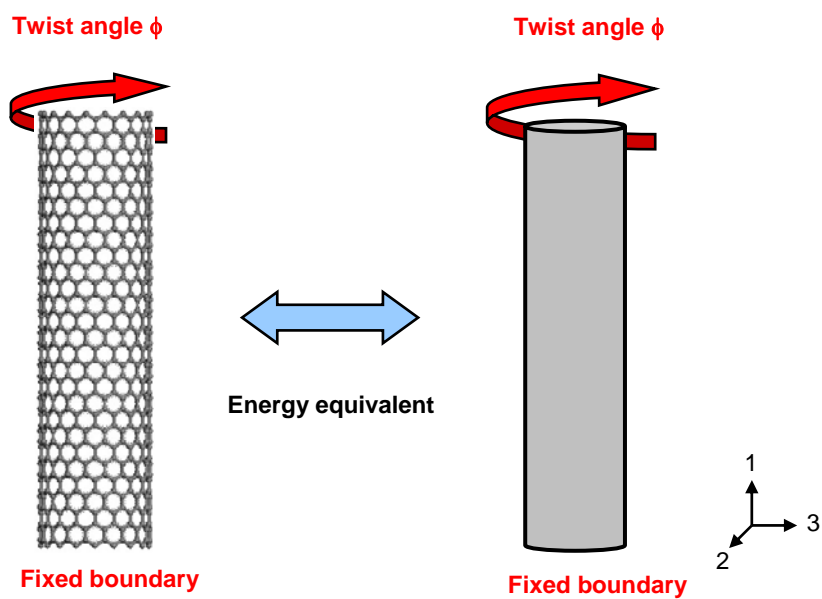
Figure 2-6. Twist deformation was applied to the SWCNTs atomistic structures and the equivalent solid cylinder.
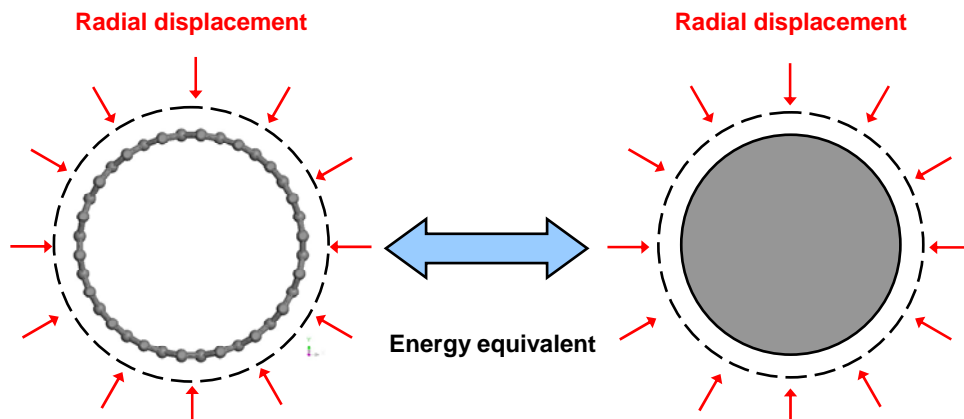
Figure 2-7. Radial deformation was applied to the SWCNTs atomistic stricture and the equivalent solid cylinder.

| (a) | (b) |
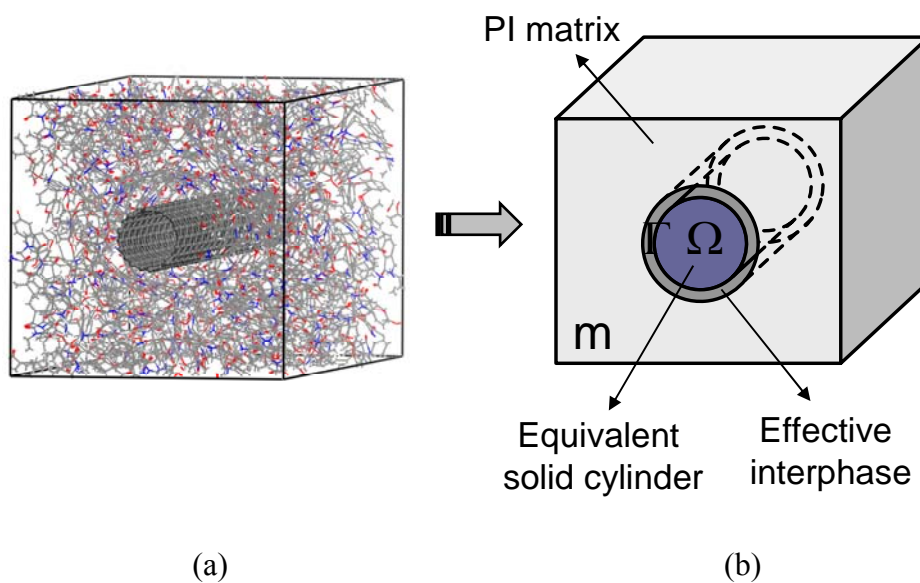
Figure 3-1. Schematic representation of simulation process: (a) SWCNTs/polyimide molecular structure and (b) three-phase micromechanical model.
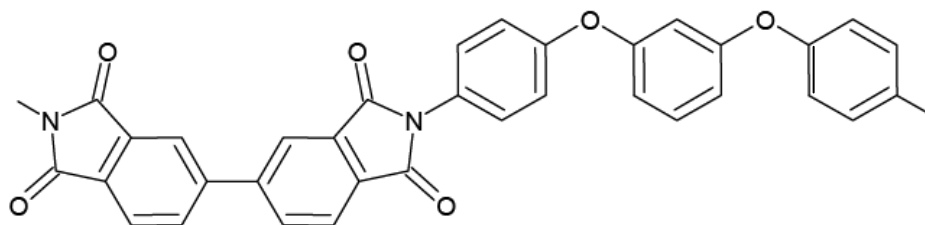
Figure 3-2. Sketch of polyimide monomer unit.
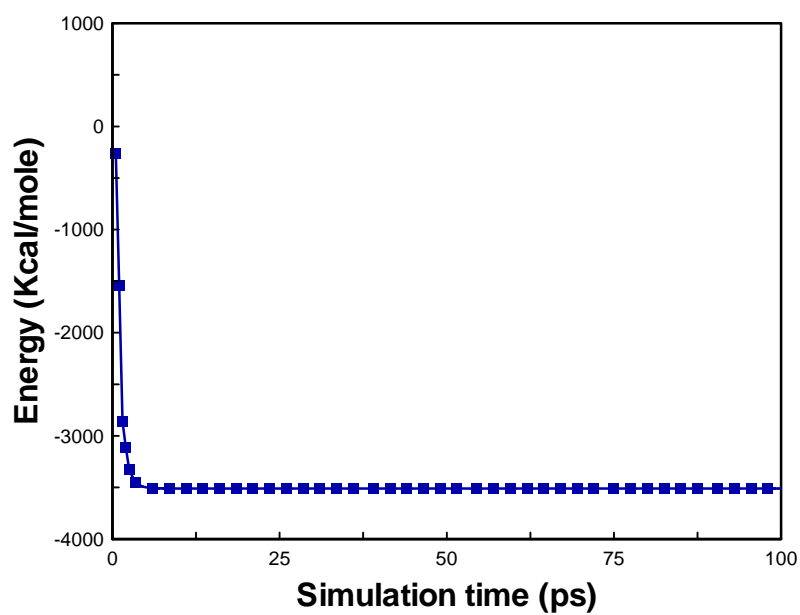
Figure 3-3. Variation of potential energy in NPT ensemble.
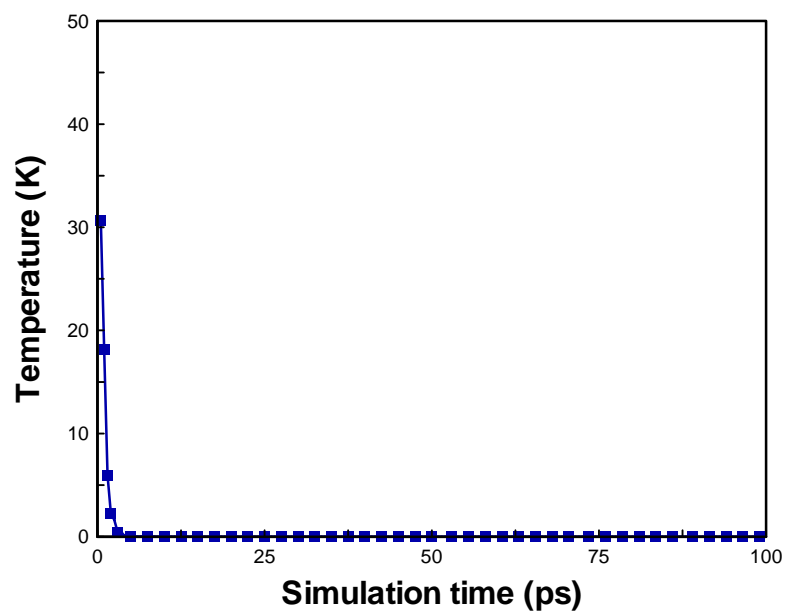
Figure 3-4. Variation of temperature in NPT ensemble.
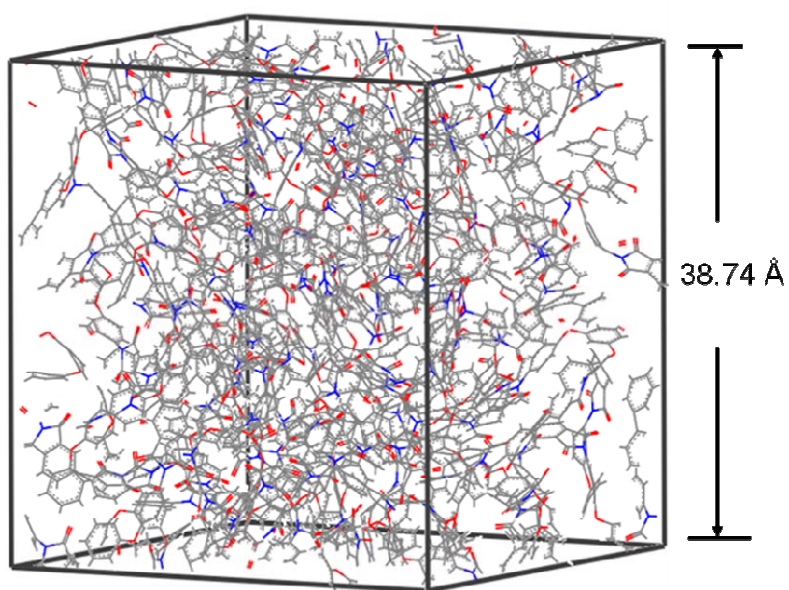
Figure 3-5. Molecular structure of polyimide polymer.
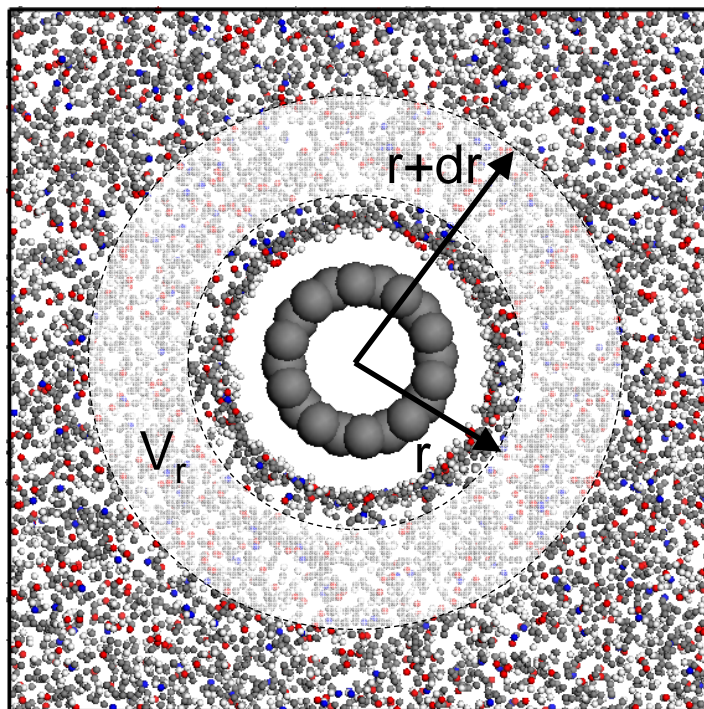
Figure 3-6. Evaluation of density distribution of polyimide polymer in the radial direction.
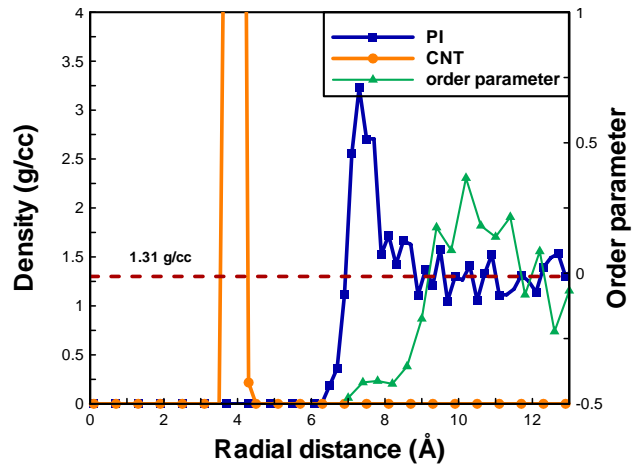
(a)
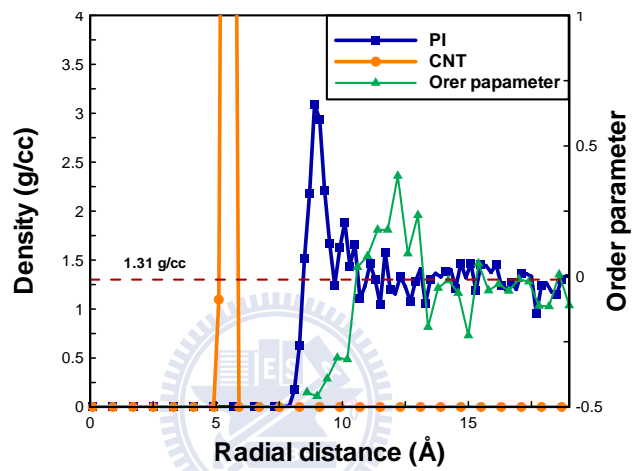
(b)
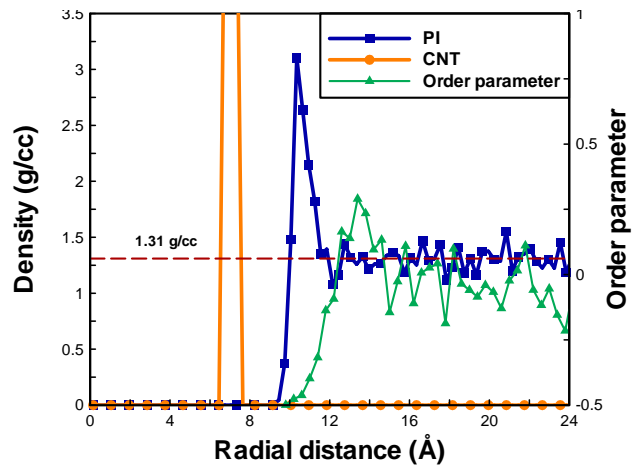
(c)

Figure 3-7. Density distribution of the SWCNTs and polyimide as well as order parameter distribution of polyimide in the radial direction with three different CNTs radii: (a) 3.9Å, (b) 5.5Å and (c) 7.1Å.
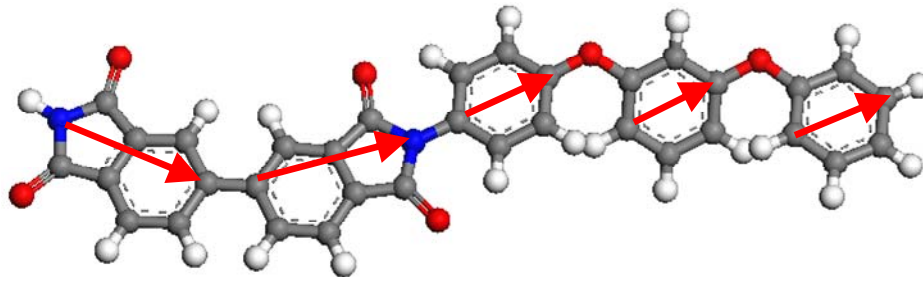
Figure 3-8. A schematic representation of the sub vector in the polyimide polymer.
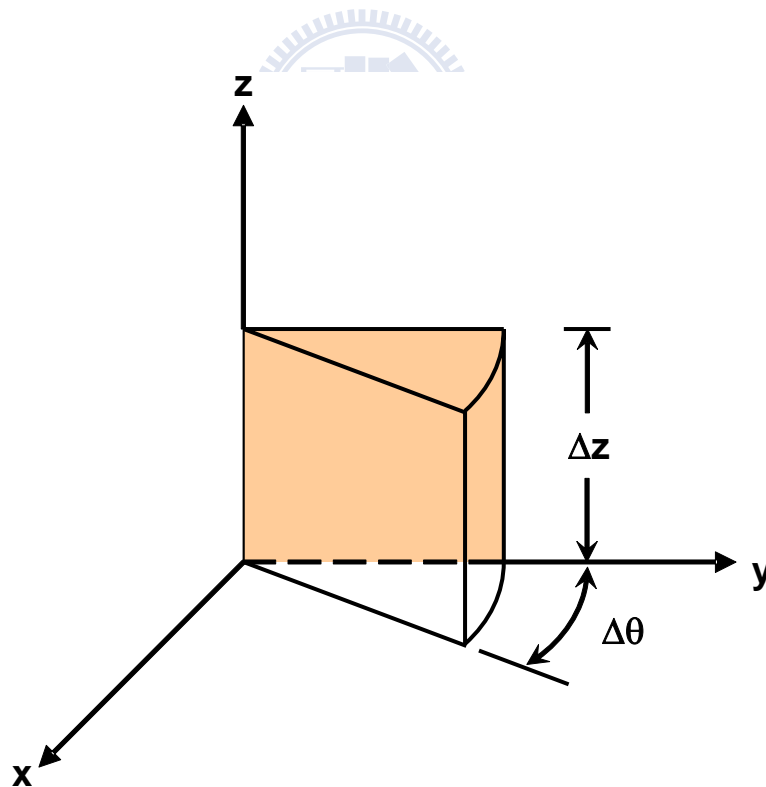
Figure 3-9. Schematic of the radial volume element for the non-bonded gap ($\Delta\theta = 10^{o}$, $\Delta z = 10\text{Å}$).
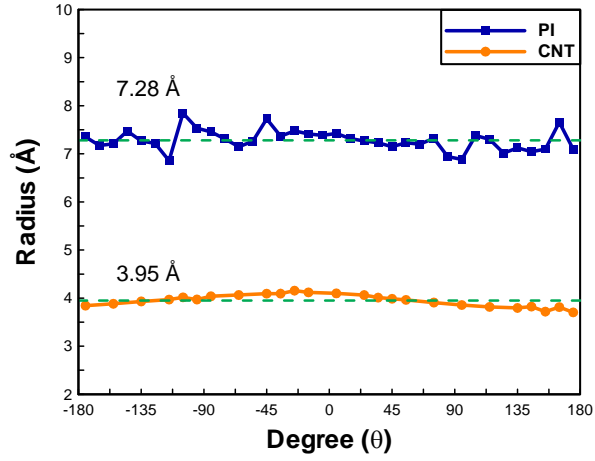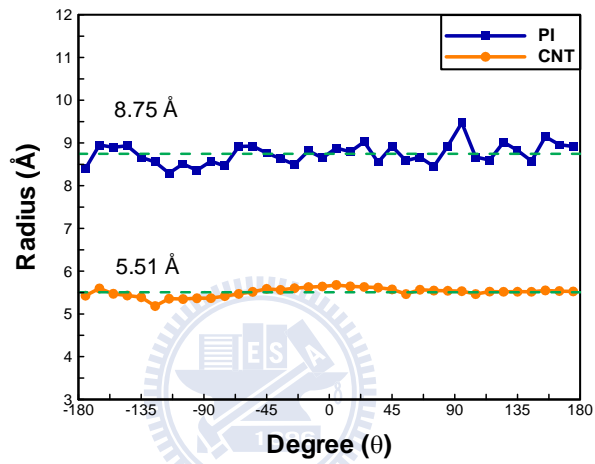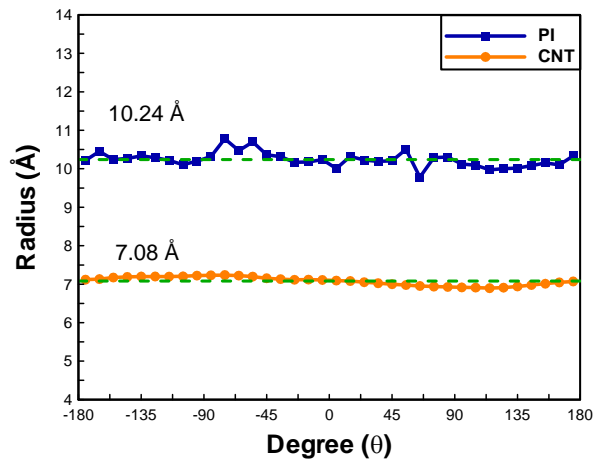
Figure 3-10. The maximum radial distance for SWCNTs atoms and the minimum radial distance for polyimide atoms within the radial volume element with three different CNT radii: (a) 3.9Å, (b) 5.5Å and (c) 7.1Å.
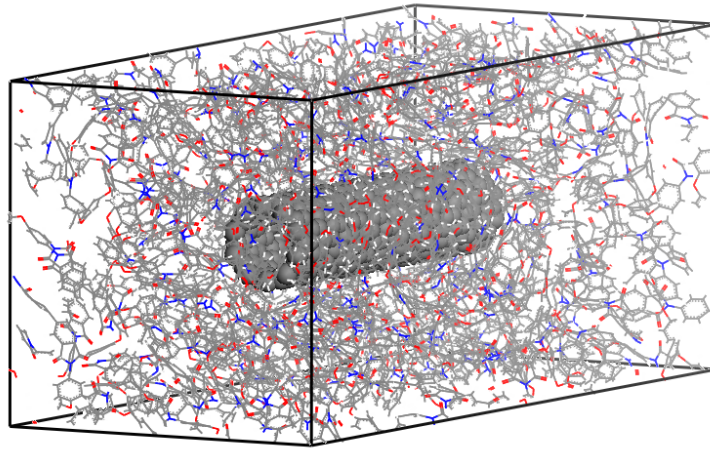
Figure 4-1. Molecular structure of SWCNTs embedded within polyimide nanocomposites.
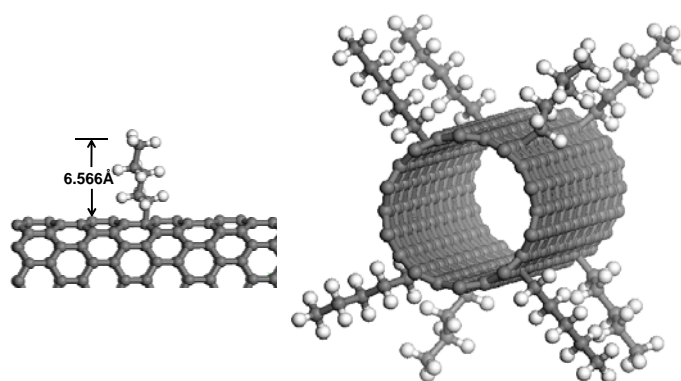
Figure 4-2. SWCNTs with surface modification of polyethylene chains.
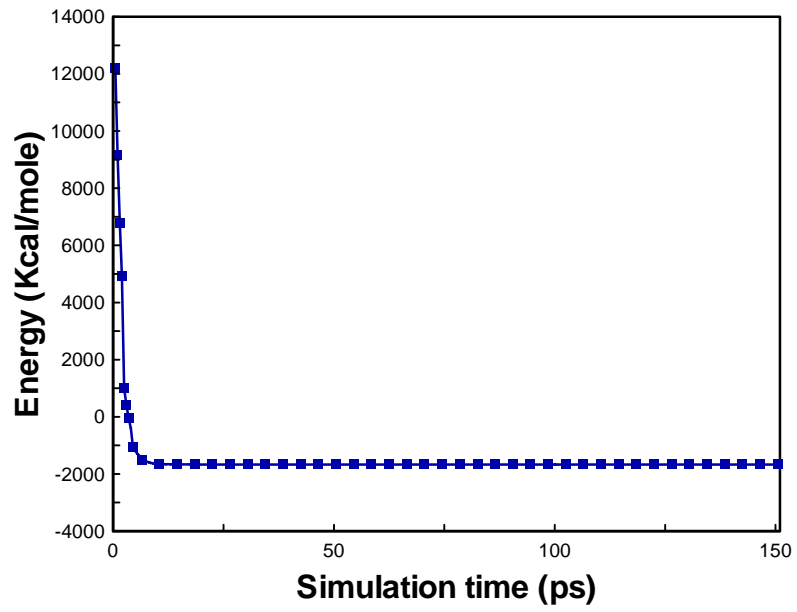
Figure 4-3. Variation of potential energy in NPT ensemble.
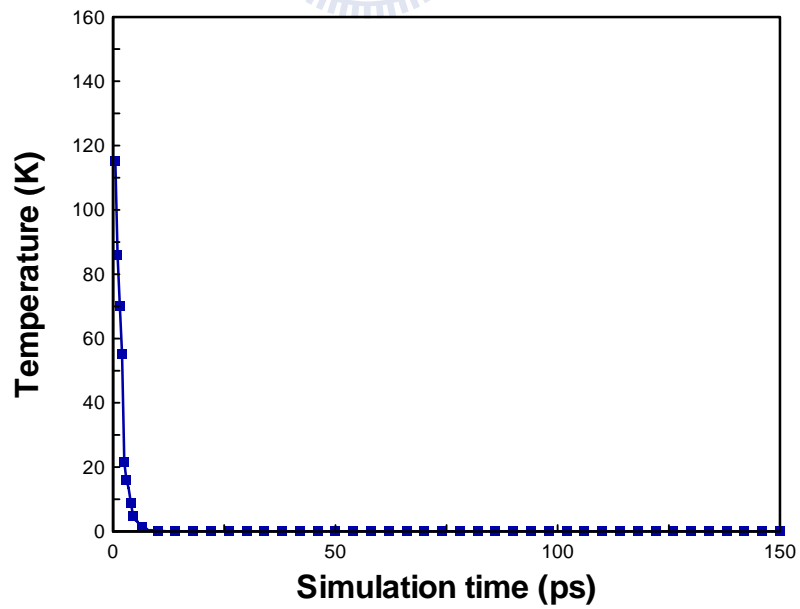
Figure 4-4. Variation of temperature in NPT ensemble.
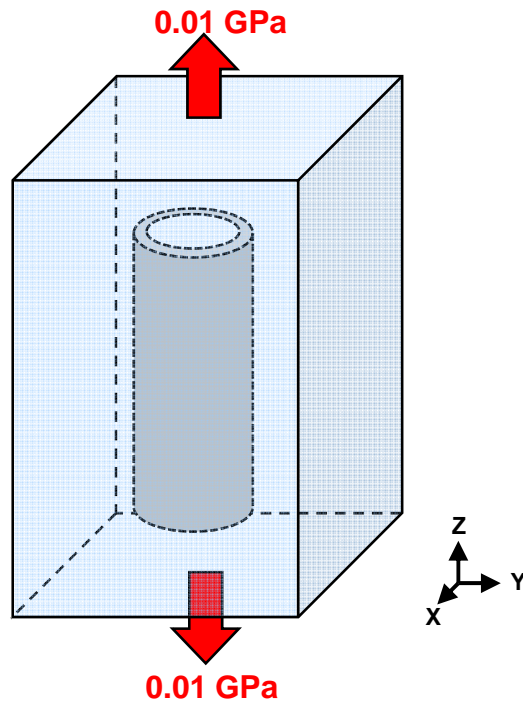
Figure 4-5. SWCNTs/polyimide nanocomposites subjected to uniaxial loading.
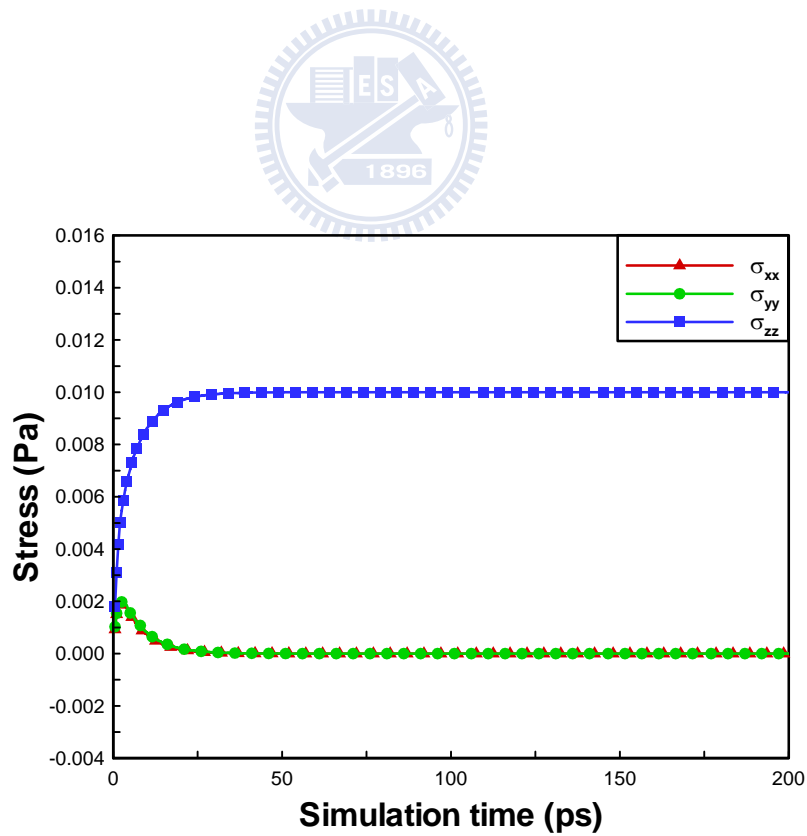
Figure 4-6. Variation of stress in modify NPT ensemble.
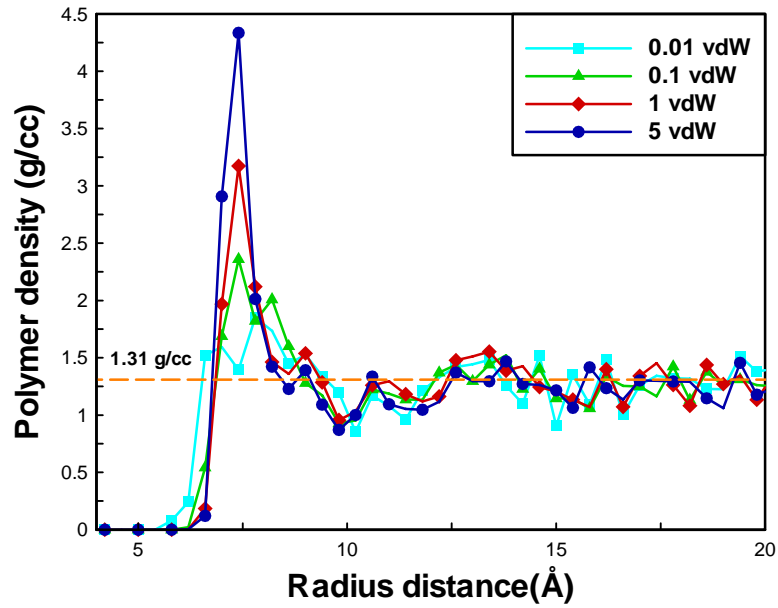
Figure 4-7. Density distribution of polyimide in the radial direction associated with four different intensities of vdW interactions.
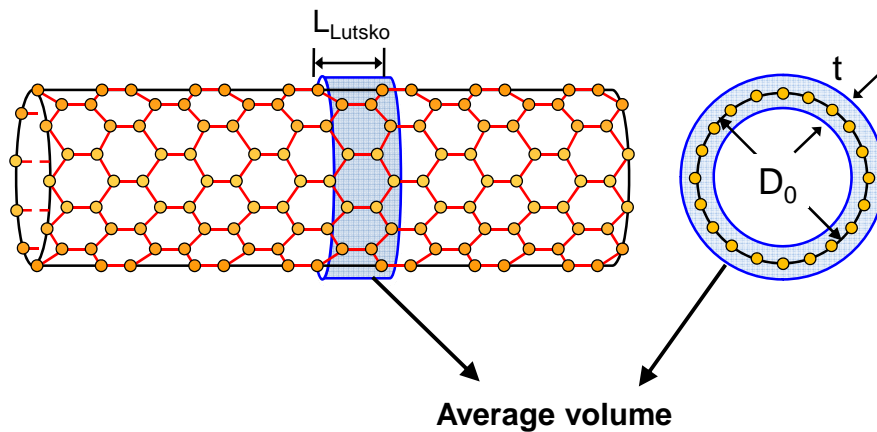
Average volume

Figure 4-8. Schematic of average volume for Lutsko stress(L_{Ltusko}=10Å, t=3.4 Å).
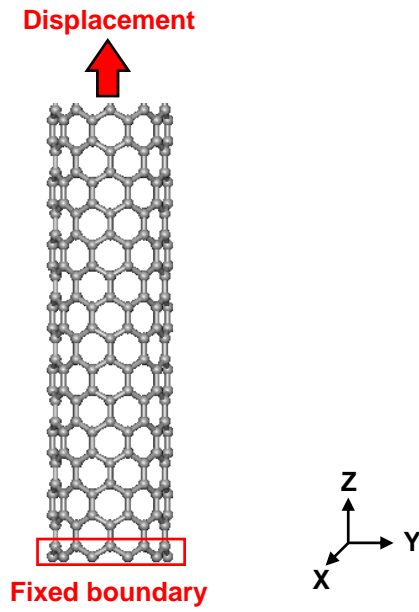
Figure 4-9. Axial deformation of SWCNTs.
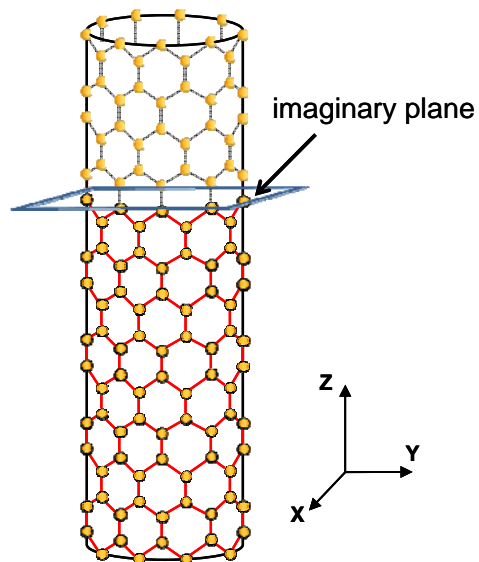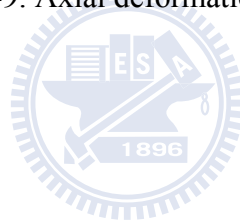
Figure 4-10. Imaginary plane assumed on the SWCNTs.
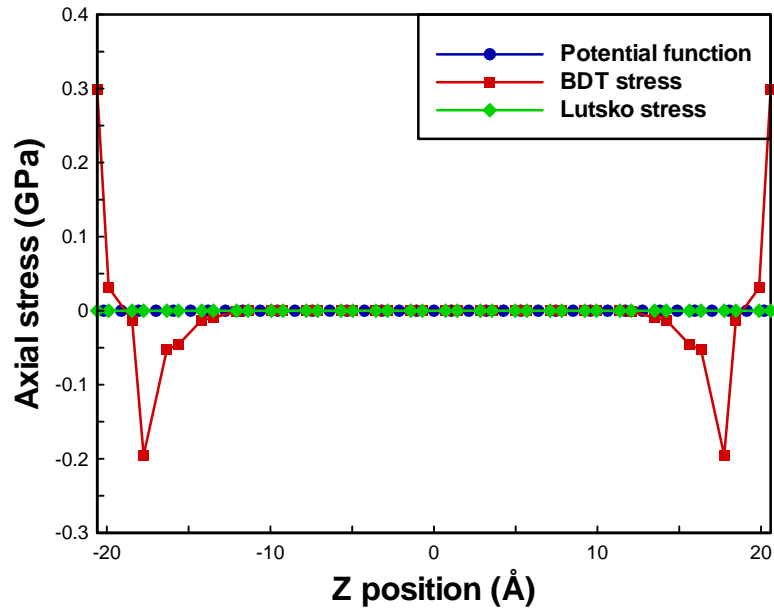
Figure 4-11. Calculation of axial stress distribution along the axial (Z) direction with stress-free state.
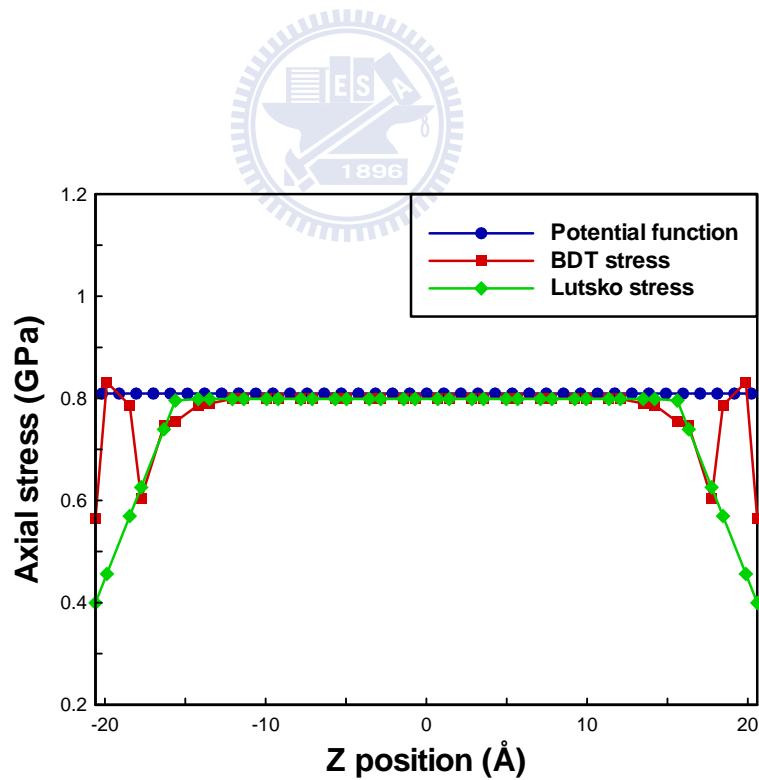
Figure 4-12. Calculation of axial stress distribution along the axial (Z) direction with uniaxial loading state.
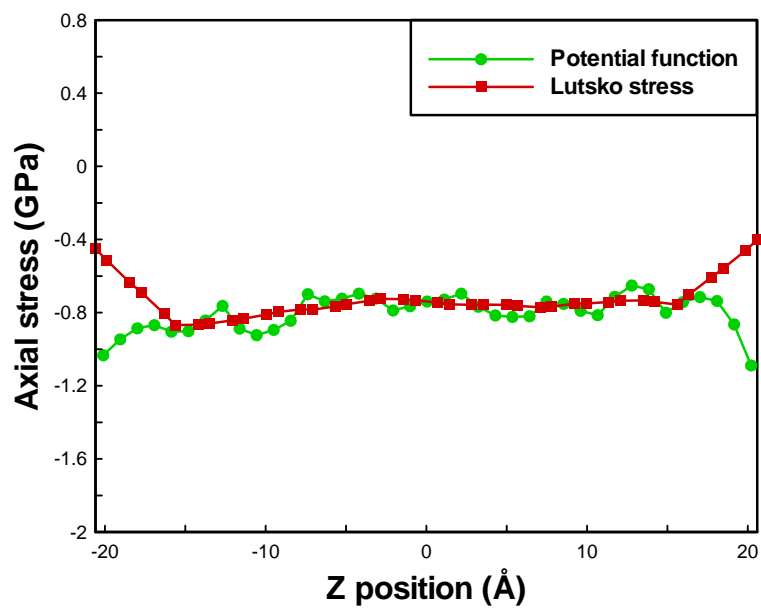
Figure 4-13. Axial stress distribution in the SWCNTs with 1 time vdW interaction at the stress-free state.
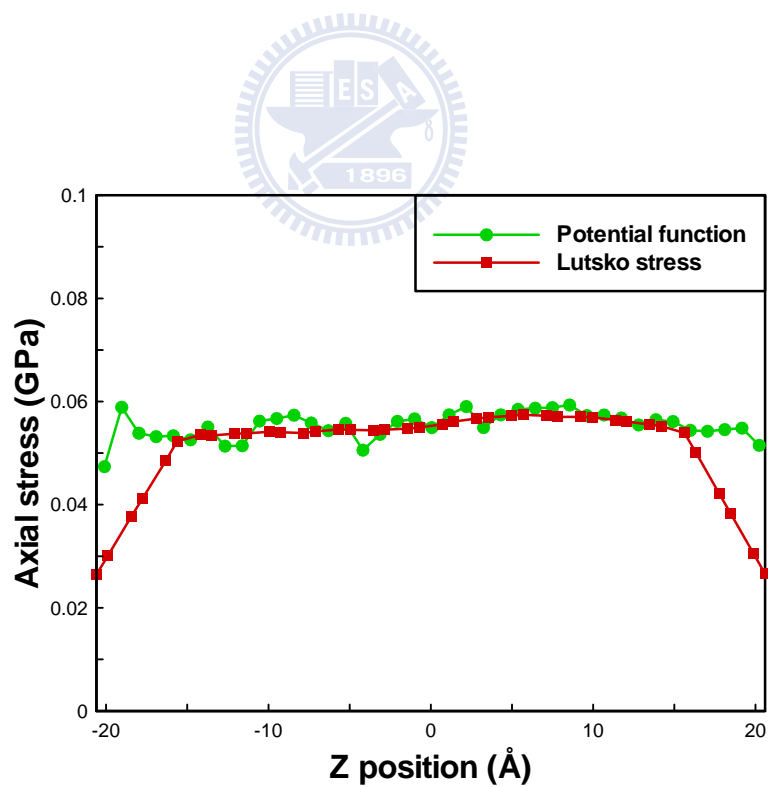
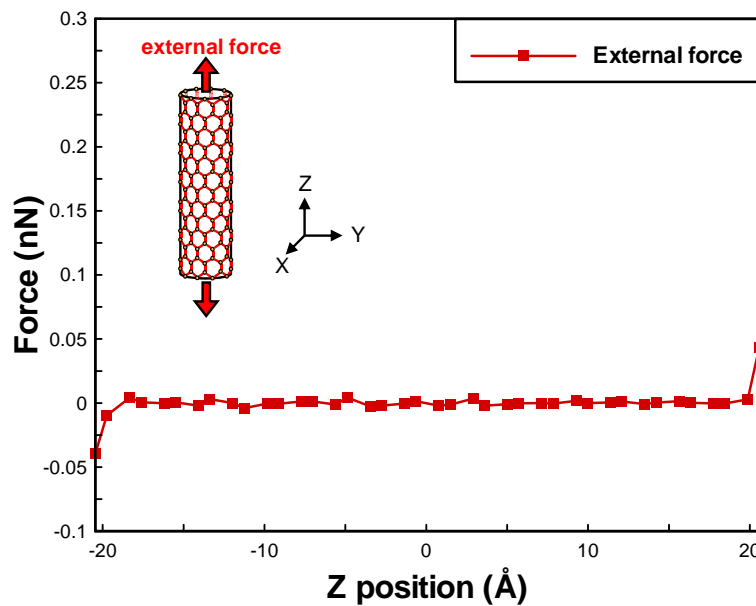Figure 4-14. Axial stress distribution in the SWCNTs with 1 time vdW interaction at the uniaxial loading state.
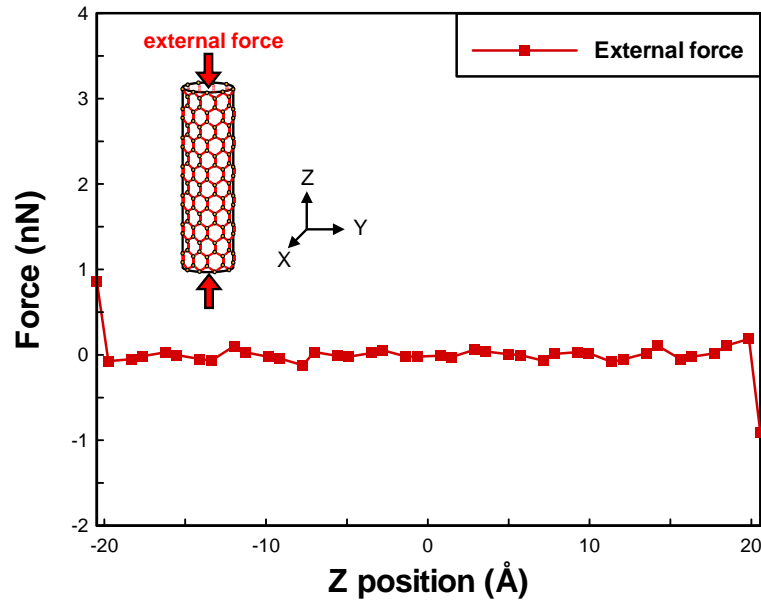
Figure 4-15. The external force distribution of SWCNTs with 1 time vdW interaction at the stress-free state.

Figure 4-16. The external force distribution of SWCNTs with 1 time vdW interaction at the uniaxial loading state.
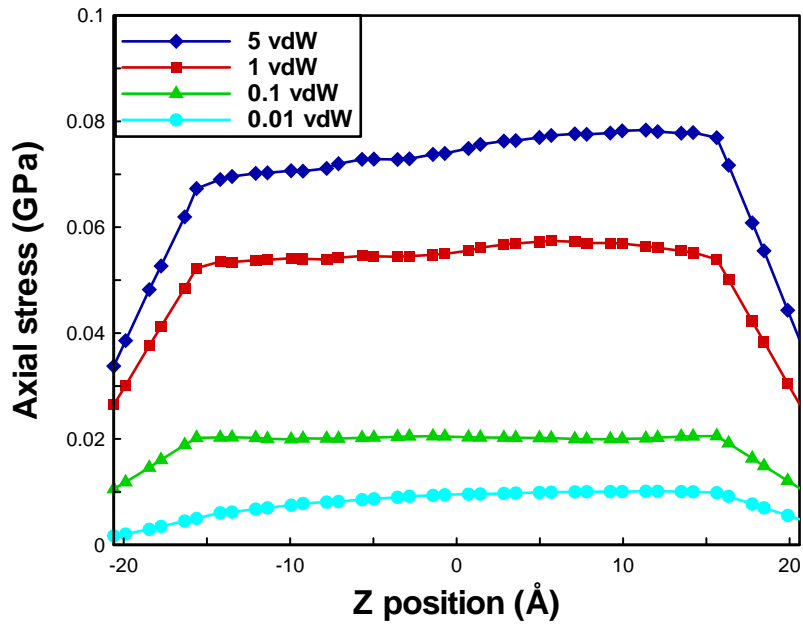
Figure 4-17. Axial stress distribution in the SWCNTs associated with four different vdW
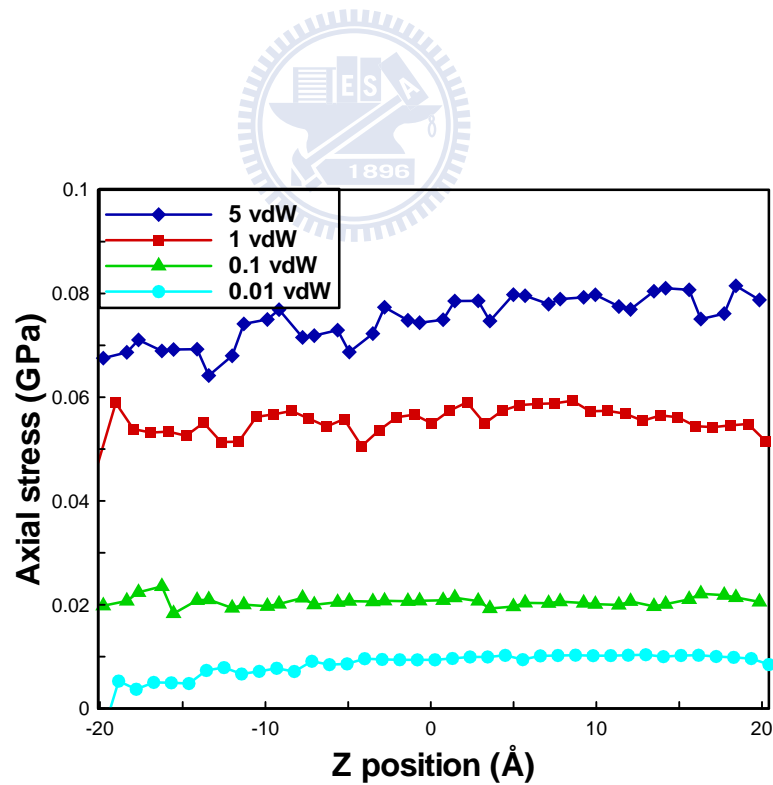interactions (Lutsko stress formulation).

Figure 4-18. Axial stress distribution in the SWCNTs associated with four different vdW
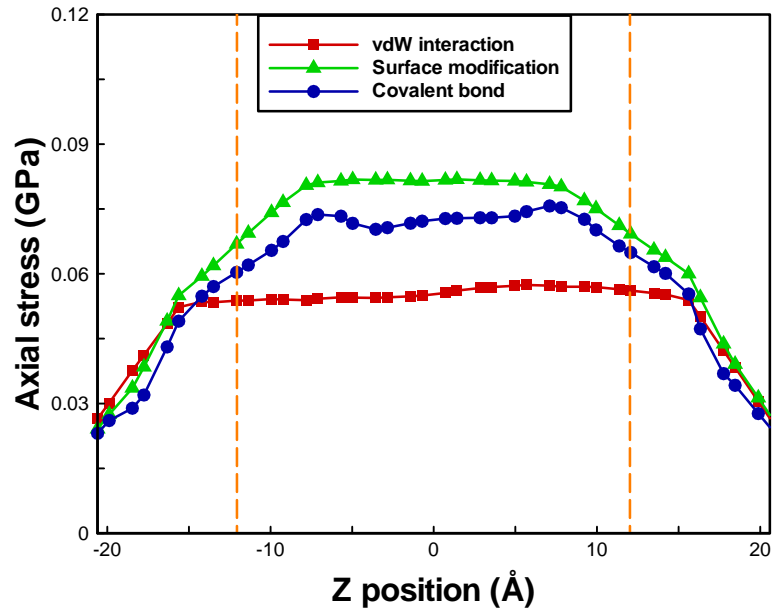interactions (Potential function).

Figure 4-19. Comparison of axial stress distribution of SWCNTs with three different interfacial adhesions (vdW interaction, surface modification and covalent bond).
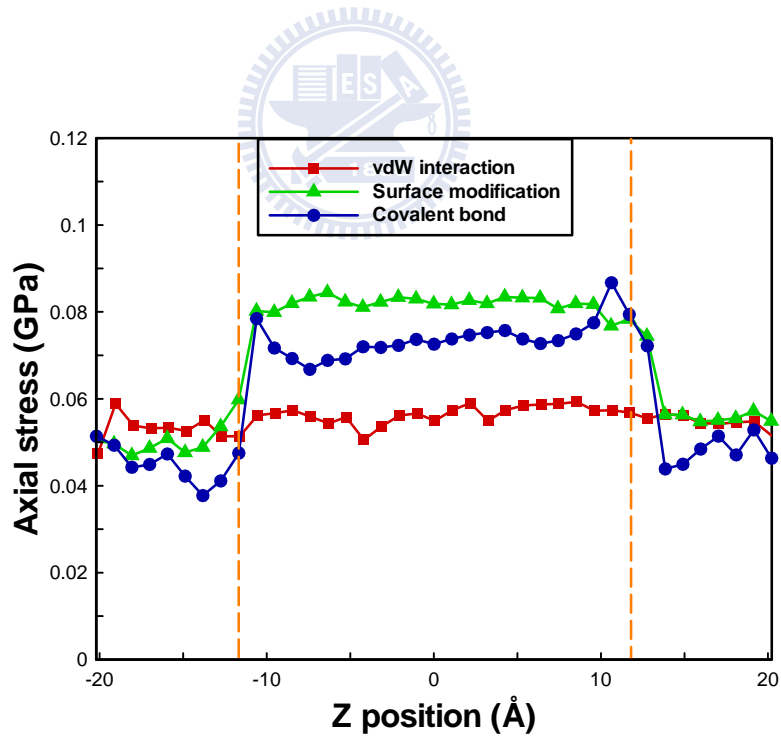

Figure 4-20. Comparison of axial stress distribution of SWCNTs with three different interfacial adhesions (vdW interaction, surface modification and covalent bond).